

cells transfected with a perlecan cDNA expression vector (Noonan et al. 1991; Costell et al. 1997; Xu et al. 2010). The full-length perlecan cDNA (Ishijima et al. 2012) was cloned into the PCEP4-Mul-PURD expression vector (Hozumi et al. 2006), which contains sequences for the CMV promoter, multiple cloning sites, BM40 signal peptide (Hozumi et al. 2006). A twenty-four well tissue culture plate was coated with rPerlecan (20 $\mu\text{g}/\text{mL}$) in PBS, including 1 mmol/L CaCl_2 and 0.5 mmol/L MgCl_2 at 4°C for 48 h. After the plate was washed twice with PBS, HAECs treated with Perlecan siRNA or Control siRNA, as described above, were plated at density of 3×10^5 cells on the Perlecan or a control plate and cultured for 36 h. The eNOS RNA expression was analyzed using qPCR.

Heparinase III digestion of HAECs

Cell surface heparan sulfate chains of HAECs were digested by heparinase III as described method (Kerever et al. 2007) with some modifications. HAECs were incubated with 5 mU/mL of heparinase III (Sigma-Aldrich, St. Louis, MO) in 50 mmol/L HEPES buffer (pH 7.0), containing 100 mmol/L NaCl and 1 mmol/L CaCl_2 at 37°C for 1 h. After the incubation, the heparinase III solution was removed and the cells were cultured with the growth media. We confirmed successful heparinase III digestion using immunostaining. A time course of the eNOS RNA expression was performed using qPCR as described above.

Immunostaining

HAECs were plated at density of 3×10^5 cells on Type-1 collagen-coated 8 well chambers and cultured for 48 h. After heparinase III digestion for 1 h, the cells were fixed immediately (time point 0) or 24 h later (time point 24 h) with 4% paraformaldehyde at room temperature. Nonspecific binding was blocked with 0.2% gelatin/PBS for 10 min and cells were incubated with anti-heparan sulfate antibody (10E4 epitope) antibody or anti- Δ heparan sulfate (3G10 epitope) antibody (Seikagaku Corporation, Tokyo, Japan) at 1:400, and anti-perlecan (clone A7L6) (Chemicon, Temecula, CA) antibody at 1:400 in 0.2% gelatin/PBS at 4°C overnight. Following a wash with PBS, the cells were incubated with goat anti-mouse IgM alexafluor 488 and goat anti-rat IgG alexafluor 546 (Molecular Probes, Invitrogen Corporation, Carlsbad, CA) at 1:400 in 0.2% gelatin/PBS for 1 h. The cells were washed and then incubated for 10 min in bis-benzimide (1:5000, Molecular Probes, Invitrogen Corporation). After extensive washes, cells were mounted in fluoro-gel with Tris buffer (Electron Microscopy Sciences, Hatfield, PA).

Images were taken using a Leica TCS-SP5 LSM confocal microscope.

Statistical analysis

The data are presented as the mean \pm SEM. Comparisons between groups were made with two-way reported measure ANOVA and with the unpaired *t*-test. A *P* value of <0.05 was considered to be statistically significant.

Results

HSPG2 deletion decreases the relaxation of mouse aorta

An endothelium-dependent relaxation of the mouse aorta was elicited by ACh. Aortic relaxation in response to ACh was significantly reduced in the *HSPG2*^{-/-}-Tg aortas compared to that of the control aortas, resulting in the downward shift of the concentration-response curve (Fig. 1A). On the other hand, the endothelium-independent relaxation elicited by exogenous nitric oxide donor

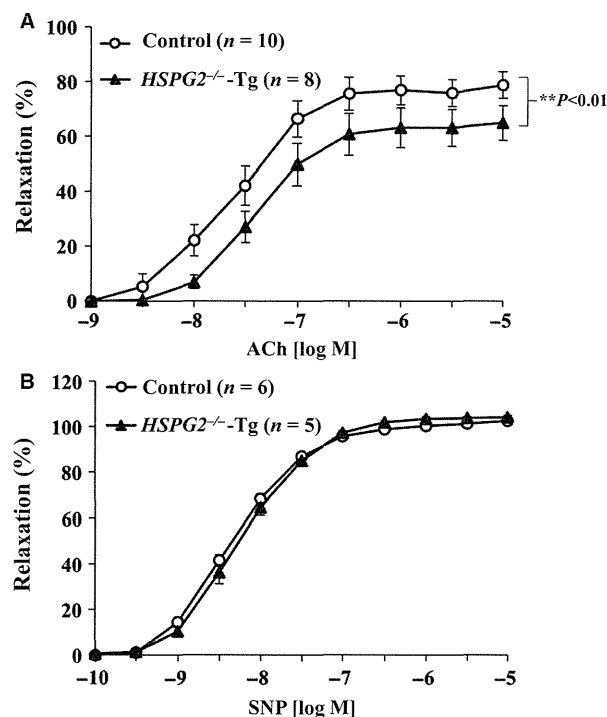


Figure 1. *HSPG2*^{-/-}-Tg aortas have a reduced relaxation in response to ACh or SNP. The aortic rings were precontracted with 1 $\mu\text{mol/L}$ phenylephrine (PE), and increasing concentrations of (A) acetylcholine (ACh) or (B) sodium nitroprusside (SNP) were added. The degree of relaxation is expressed as the percent relaxation of the PE-induced tone (The bars indicate the mean \pm SEM, *n* = 5–10).

SNP was not affected by the deletion of *HSPG2*, as shown in Figure 1B, indicating that the sensitivity of vascular smooth muscle to exogenous nitric oxide donors is well preserved, even in *HSPG2*^{-/-}-Tg aortas.

HSPG2 deletion decreases the expression level of eNOS in mouse aortas

We explored the mechanisms underlying the reduction of endothelium-dependent relaxation by measuring RNA expression levels of both eNOS and von Willebrand factor (vWF), an endothelial cell specific gene, using qPCR. RNA was extracted from aortic tissue from control and from *HSPG2*^{-/-}-Tg animals. The vWF expression level in the control and in the *HSPG2*^{-/-}-Tg aortas was not significantly different (Fig. 2A). However, qPCR analysis revealed that eNOS mRNA expression was significantly reduced in the *HSPG2*^{-/-}-Tg aortas (Fig. 2B). We also measured protein expression levels of eNOS in the control and in the *HSPG2*^{-/-}-Tg aortas by Western blotting. The protein level of eNOS was significantly decreased in the *HSPG2*^{-/-}-Tg aortas compared with that of the control aortas (Fig. 2C). These results indicated that eNOS expression was decreased in the perlecan-deficient aortas.

eNOS expression was decreased in HAECs by Perlecan siRNA treatment

We examined the relationship between eNOS expression and perlecan expression by creating perlecan knockdown HAECs in culture using Perlecan siRNA treatment. We measured the RNA expression levels by qPCR using RNA extracted from HAECs treated with control or Perlecan siRNA. We confirmed that perlecan mRNA expression levels in HAECs were significantly decreased by approximately 90% following treatment with both 20 and 40 nmol of Perlecan siRNA (Fig. 3A). The eNOS mRNA expression was significantly decreased by approximately 50% following Perlecan siRNA treatment (Fig. 3B). These results indicated that reduced perlecan expression decreases eNOS expression in HAECs.

Depletion of heparan sulfate chains does not affect the eNOS expression

We performed enzymatic depletion of the heparan sulfate chains of perlecan on HAECs to explore whether heparan sulfate chains are critical for eNOS expression. The time course of the experimental protocol is shown in Figure 4A. First, we confirmed the depletion of heparan

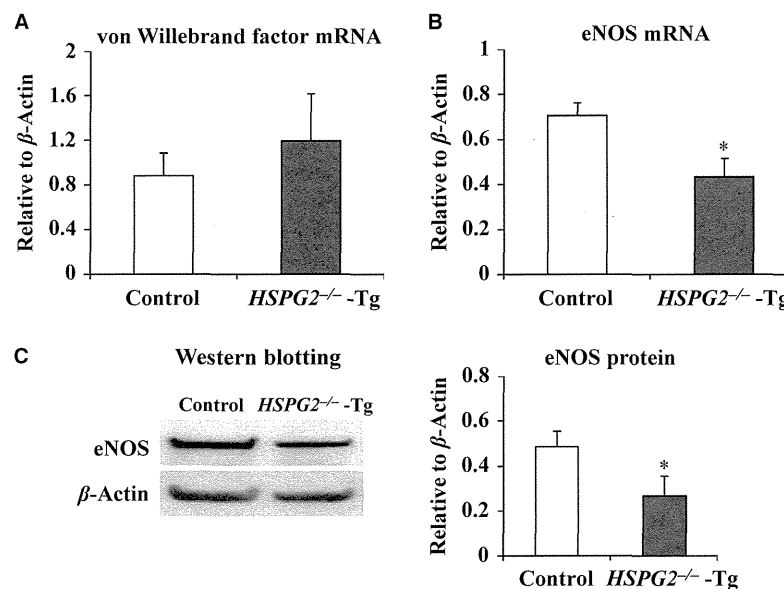


Figure 2. Expression of endothelial nitric oxide synthase (eNOS) in the *HSPG2*^{-/-}-Tg aorta. RNA expression levels of von Willebrand factor and eNOS in the aortic tissues of 10 week control and *HSPG2*^{-/-}-Tg mice were analyzed using qPCR. (A) The expression of von Willebrand factor was not significantly different, while (B) eNOS expression was significantly reduced in the *HSPG2*^{-/-}-Tg animals ($n = 6$ per genotype). The bars indicate the mean \pm SEM). RNA expressions levels were normalized to that of β -actin and were indicated as relative to β -actin. (C) The protein expression levels of eNOS and β -actin in the aortic tissues were evaluated, using Western blotting. Each band was quantified using ImageJ software and is shown as relative to β -actin. The protein expression levels of eNOS were significantly decreased in the *HSPG2*^{-/-}-Tg mice compared to that in the control mice ($n = 4$ per genotype). The bars indicate the mean \pm SEM). * $P < 0.05$ versus control mice.

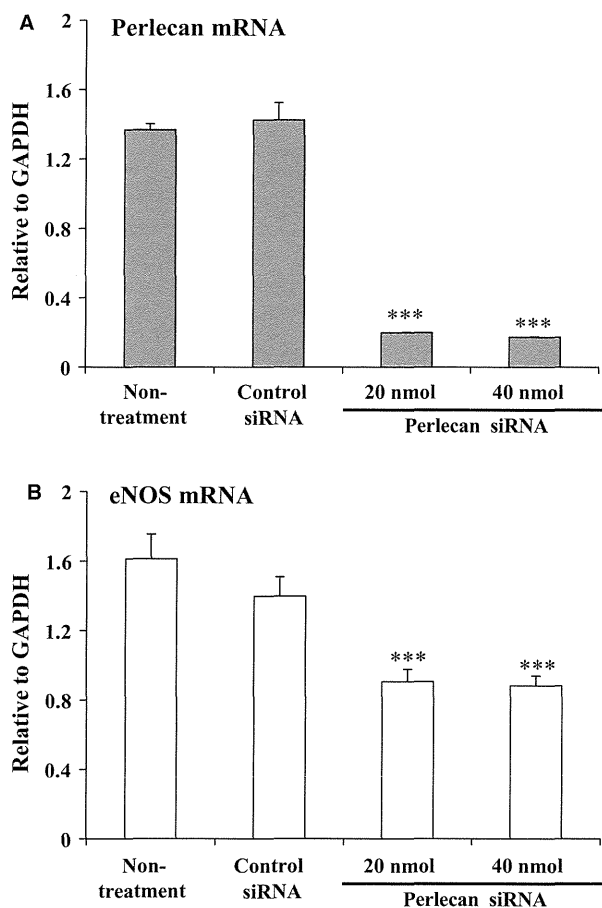


Figure 3. RNA expression of eNOS in human aortic endothelial cells (HAECs) treated with *HSPG2* siRNA. Analyses of perlecan and eNOS RNA expression levels in the HAECs treated with or without control siRNA and 20 or 40 nmol of Perlecan siRNA using qPCR. RNA expressions were normalized to that of GAPDH and are indicated as relative to GAPDH. (A) Perlecan expression in HAECs was significantly decreased by approximately 90% following Perlecan siRNA treatment. (B) eNOS expression showed a significant decrease of approximately 50% following treatment with Perlecan siRNA. The bars indicate the mean \pm SEM ($n = 3$), *** $P < 0.001$ versus control cells.

sulfate chains in HAECs by immunostaining using 10E4 and 3G10 antibodies. After heparinase III treatment for 1 h (time point 0), the staining by 10E4 antibody (green), which is directed against heparan sulfate chains, was not detected (Fig. 4Ba and Bc) and the staining by 3G10 antibody (green), which is directed against heparinase-generated HS stubs, was detected in the treated but not untreated HAECs (Fig. 4Bb and Bd). Similar results were obtained after 24 h (time point 24 h) (Fig. 4Be–Bh). In these conditions, we analyzed eNOS expression by qPCR at 1, 12, and 24 h after heparinase III treatment for 1 h. The eNOS expression levels in the heparinase treated

HAECs were not different compared with that of the non-treated HAECs at any time point (Fig. 4C). These results suggest that the decrease of eNOS expression in perlecan-deficient aortas is not due to the heparan sulfate chains.

Perlecan protein is necessary for eNOS expression

In order to explore whether perlecan protein is critical for eNOS expression, we performed perlecan rescue experiments using recombinant perlecan protein (rPerlecan). HAECs treated with Perlecan siRNA or Control siRNA were seeded on plates coated with or without rPerlecan. After 36 h, the eNOS expression level was analyzed by qPCR. First, we confirmed that the eNOS expression level in HAECs treated with Perlecan siRNA was significantly decreased compared with that of Control siRNA. However, the eNOS expression level in HAECs treated with Perlecan siRNA was restored to the level almost similar to that in HAECs treated with Control siRNA by rPerlecan (Fig. 5). These results suggest that perlecan is responsible for the decrease in eNOS expression in perlecan-deficient aortas.

Discussion

In the present study, we showed that a deficiency of perlecan results in the impairment of endothelium-dependent vascular relaxation in mice aorta, whereas endothelium-independent relaxation in response to the nitric oxide donor SNP remained well preserved. We investigated the mechanism(s) underlying the reduction in endothelium-dependent relaxation by examining the eNOS expression levels in aortic tissue and found that both eNOS mRNA and protein levels were decreased in the perlecan-null aortas. We further examined the relationship between perlecan deficiency and a decreased eNOS expression by treating HAECs with perlecan siRNA and found that a reduction in the perlecan gene expression induced a decrease in eNOS gene expression. This is the first report to show that perlecan deficiency results in a reduction in endothelium-dependent relaxation due, at least partly, to a decrease in eNOS expression. Although perlecan has been implicated in vascular development, the function of VSMCs with respect to relaxation is not affected by the deletion of the perlecan gene, suggesting a lesser contribution of perlecan in VSMCs than in endothelial cells.

NO is a gaseous lipophilic free radical generated by constitutively expressed eNOS in vascular endothelial cells (Braam and Verhaar 2007). The expression levels of eNOS are altered in patients with various pathophysiological

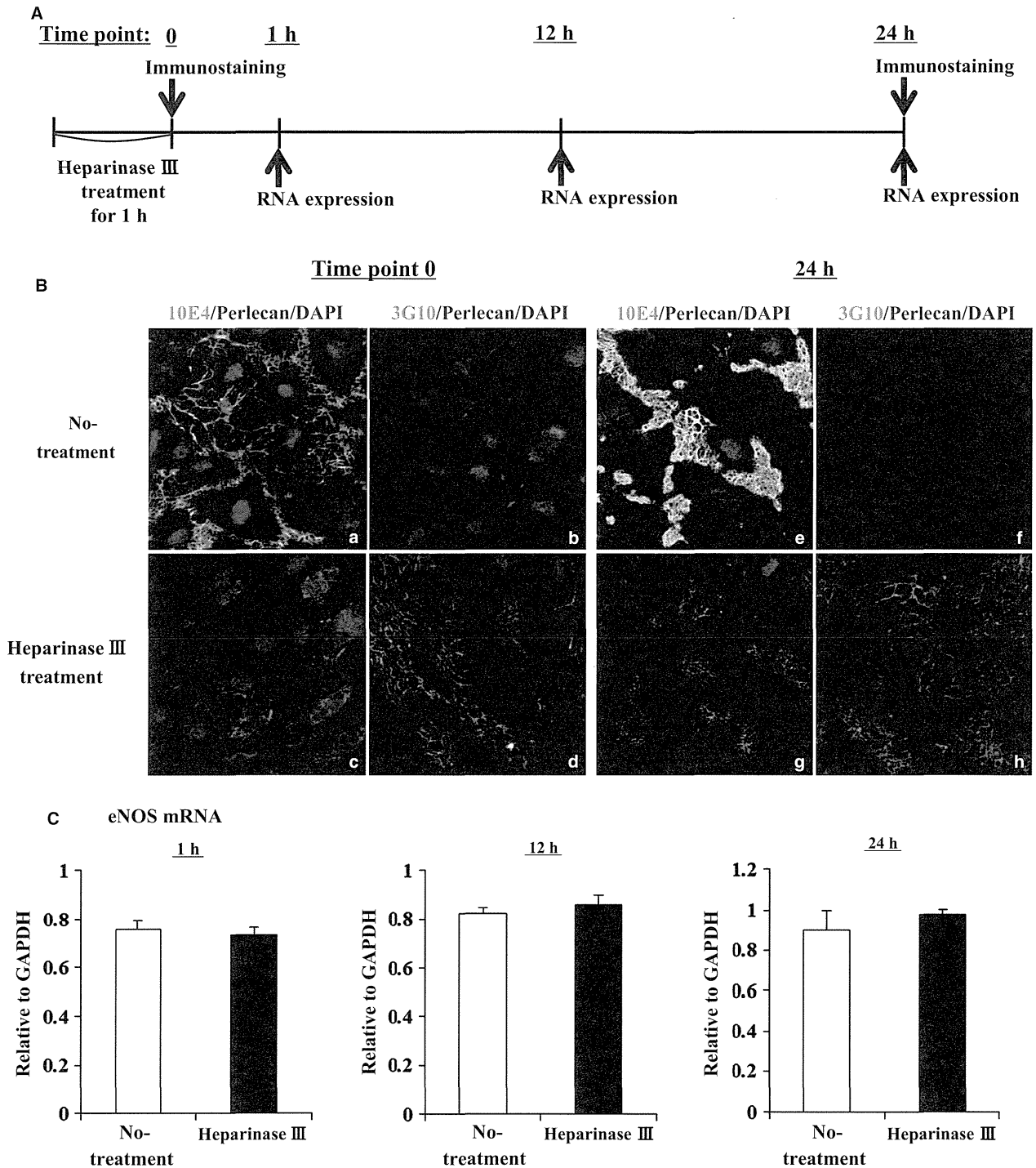


Figure 4. RNA expression levels of eNOS in HAECs treated with heparinase III. (A) A time course of experimental protocol using heparinase III. (B) The heparan sulfate chains were removed from HAECs using heparinase III. After a 1 h treatment with or without heparinase III, the cells were fixed immediately (time point 0) or 24 h later (time point 24 h), and immunostaining was performed with 10E4 or 3G10 (Green), and perlecan (Red) antibodies. Successful heparinase III digestion is indicated by negative staining of 10E4 (c and g) and positive staining of 3G10 (d and h). At 24 h culture after heparinase III treatment, heparan sulfate chains were not detected (g and h). (C) Analysis of eNOS RNA expression levels in HAECs treated with or without heparinase III using qPCR. eNOS RNA expressions was normalized to that of GAPDH and it is indicated as relative to GAPDH. eNOS expression levels in the heparinase III treated HAECs was not significantly different compared with that of the non-treated HAECs at 1, 12, and 24 h later. The bars indicate the mean ± SEM ($n = 3$)

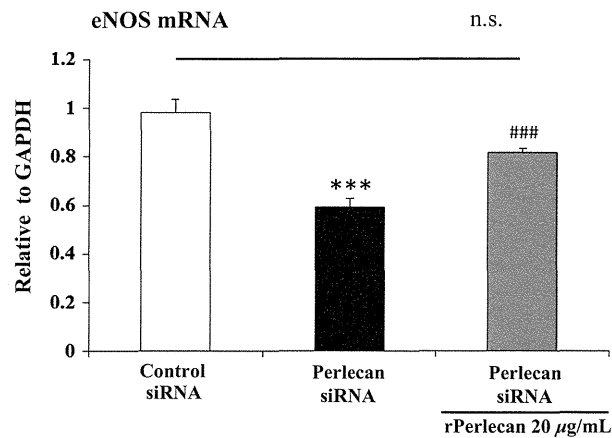


Figure 5. RNA expression level of eNOS in Perlecan knockdown HAECs on perlecan recombinant protein. qPCR analysis of eNOS RNA expression level in HAECs treated with Perlecan or Control siRNA and seeded on a plate coated with or without perlecan recombinant protein (rPerlecan). The level of the eNOS RNA expression was normalized to that of GAPDH and it is indicated as relative to GAPDH. The eNOS expression level in HAECs treated with Perlecan siRNA was significantly decreased compared to that of Control siRNA treated HAECs. HAECs treated with Perlecan siRNA and plated on rPerlecan was no significantly different compared with that of Control siRNA treated HAECs. The bars indicate the mean \pm SEM ($n = 4$) *** $P < 0.001$ versus Control siRNA treated HAECs without rPerlecan, ### $P < 0.001$ versus Perlecan siRNA treated HAECs without rPerlecan.

conditions, such as cardiovascular disease, atherosclerosis, diabetes mellitus, and hypertension (Chatterjee et al. 2008). The transcriptional activation of the eNOS gene is stimulated by shear stress (Papapetropoulos et al. 1999), exercise (Sessa et al. 1994), and the action of lysophosphatidylcholine (Zembowicz et al. 1995) and several growth factors, including VEGF (Bouloumie et al. 1999), bFGF, and epidermal growth factor (EGF) (Braam and Verhaar 2007). Conversely, eNOS expression is down-regulated by tumor necrosis factor- α (TNF- α) (Nishida et al. 1992), hypoxia (McQuillan et al. 1994), and high concentrations of low-density lipoprotein (LDL) (Laufs et al. 1998). eNOS activity at the post-translational level is regulated by several mechanisms, including interactions with other proteins, acylation, phosphorylation, and cellular localization (Braam and Verhaar 2007). In the present study, we demonstrated that perlecan plays a role in endothelium-dependent vascular relaxation, acting in part through maintenance of the eNOS expression levels.

Proliferation of endothelial cells requires multiple growth factors, including VEGF and FGF-2 (Carmeliet 2000; Iozzo and San Antonio 2001), which elicit their activities by binding to HSPGs in the vascular wall (Iozzo

and San Antonio 2001). These growth factors must bind to HSPGs in the vascular wall in order to function stably (Iozzo and San Antonio 2001). These growth factors also upregulate eNOS expression (Braam and Verhaar 2007), therefore it is conceivable that perlecan deficiency results in reduced binding of growth factors to the vessel wall, thereby reducing eNOS expression. The expression of vWF, another marker of endothelial cells, was not affected by perlecan deficiency in this study, suggesting that the reduction in eNOS expression is rather specific to perlecan deficiency. Perlecan binds to several growth factors, including VEGF and FGF-2, via its HS chains (Zoeller et al. 2009). Perlecan from endothelial cells and the recombinant endorepellin protein, a C-terminal fragment of perlecan, binds to VEGFR-1 and -2, and modulate the VEGF-VEGFR signaling pathway in endothelial cells (Goyal et al. 2011; Ishijima et al. 2012). In this study, we showed that the depletion of heparan sulfate chains did not affect the eNOS expression level in HAECs. On the other hand, the eNOS expression level of HAECs treated with Perlecan siRNA was restored to the similar level of Control siRNA in the presence of recombinant perlecan protein. These results suggest that the decrease in the eNOS expression level in perlecan knockout aorta is due to the deficiency of the perlecan core protein. The precise mechanisms that underlie this reduced eNOS expression induced by perlecan deficiency remain to be elucidated. However, this study is the first, to our knowledge, to show a direct relationship between perlecan deficiency and a reduction in eNOS mRNA expression.

We previously reported that heterozygous deficiency of perlecan results in a reduced rate of atherosclerosis in apoE null mice (Vikramadithyan et al. 2004), suggesting that perlecan possesses pro-atherosclerotic properties. In addition, perlecan heparan sulfate (HS) chains promote atherosclerosis, as the depletion of endogenous perlecan HS was associated with a reduced frequency of atherosclerosis in apoE null mice (Tran-Lundmark et al. 2008), again suggesting that perlecan is pro-atherosclerotic. In contrary, our results suggest that the perlecan protein plays an atheroprotective role by activating the expression of eNOS during the normal growth process. The discrepancy in these results may be due to the differences in the animal models used and the time points of observation in each study, as the formation of atherosclerotic lesions is a chronic process that includes multiple steps of progression over several weeks. In the present study, we examined the role of perlecan in normal growth, not in animals exposed to atherosclerotic stimuli.

We previously investigated the effects of perlecan deletion on several adult organs in mice, including skeletal muscle (Xu et al. 2010), corneal epithelial tissues (Inomata

et al. 2012), endochondral bone formation (Ishijima et al. 2012), and synovial joints in the setting of knee osteoarthritis (Kaneko et al. 2013). Taken together, the results suggested that perlecan plays diverse roles in supporting tissues and homeostasis of tissue functions. In the present study, we found that the deletion of perlecan resulted in endothelial dysfunction, which is a new and rather unexpected finding, despite previous reports indicating that perlecan plays a role in the development of the cardiovascular system (Costell et al. 2002). This finding may indicate a potential cardiovascular risk in patients with Schwartz–Jampel syndrome, a disease caused by mutations in the perlecan gene in humans (Nicole et al. 2000; Arikawa-Hirasawa et al. 2002; Stum et al. 2006).

In conclusion, we showed that deficiency of perlecan led to endothelial dysfunction, as represented by a reduction in endothelium-dependent relaxation, which is thought to constitute the very early phase of atherosclerosis (Vanhoutte 2009). This dysfunction was due, at least partly, to a reduction in eNOS expression, indicating that perlecan plays a role in the activation of eNOS gene expression during normal growth.

Acknowledgments

We specially thank Dr. Y. Yamada for valuable advice, and Dr. Z. Xu, Dr. N. Liang, Dr. A. Kerever, Dr. T. Nakamura, and Dr. K. Sumiyoshi for the mouse management and technical assistance.

Conflict of Interest

None declared.

References

- Arikawa-Hirasawa, E., H. Watanabe, H. Takami, J. R. Hassell, and Y. Yamada. 1999. Perlecan is essential for cartilage and cephalic development. *Nat. Genet.* 23:354–358.
- Arikawa-Hirasawa, E., W. R. Wilcox, A. H. Le, N. Silverman, P. Govindraj, J. R. Hassell, et al. 2001. Dyssegmental dysplasia, Silverman-Handmaker type, is caused by functional null mutations of the perlecan gene. *Nat. Genet.* 27:431–434.
- Arikawa-Hirasawa, E., A. H. Le, I. Nishino, I. Nonaka, N. C. Ho, C. A. Francomano, et al. 2002. Structural and functional mutations of the perlecan gene cause Schwartz–Jampel syndrome, with myotonic myopathy and chondrodysplasia. *Am. J. Hum. Genet.* 70:1368–1375.
- Bonetti, P. O., S. H. Wilson, M. Rodriguez-Porcel, D. R. Jr Holmes, L. O. Lerman, and A. Lerman. 2002. Simvastatin preserves myocardial perfusion and coronary microvascular permeability in experimental hypercholesterolemia independent of lipid lowering. *J. Am. Coll. Cardiol.* 40:546–554.
- Bouloumie, A., V. B. Schini-Kerth, and R. Busse. 1999. Vascular endothelial growth factor up-regulates nitric oxide synthase expression in endothelial cells. *Cardiovasc. Res.* 41:773–780.
- Braam, B., and M. C. Verhaar. 2007. Understanding eNOS for pharmacological modulation of endothelial function: a translational view. *Curr. Pharm. Des.* 13:1727–1740.
- Cai, H., and D. G. Harrison. 2000. Endothelial dysfunction in cardiovascular diseases: the role of oxidant stress. *Circ. Res.* 87:840–844.
- Carmeliet, P. 2000. Mechanisms of angiogenesis and arteriogenesis. *Nat. Med.* 6:389–395.
- Chatterjee, A., S. M. Black, and J. D. Catravas. 2008. Endothelial nitric oxide (NO) and its pathophysiological regulation. *Vascul. Pharmacol.* 49:134–140.
- Costell, M., K. Mann, Y. Yamada, and R. Timpl. 1997. Characterization of recombinant perlecan domain I and its substitution by glycosaminoglycans and oligosaccharides. *Eur. J. Biochem.* 243:115–121.
- Costell, M., E. Gustafsson, A. Aszodi, M. Morgelin, W. Bloch, E. Hunziker, et al. 1999. Perlecan maintains the integrity of cartilage and some basement membranes. *J. Cell Biol.* 147:1109–1122.
- Costell, M., R. Carmona, E. Gustafsson, M. Gonzalez-Iriarte, R. Fassler, and R. Munoz-Chapuli. 2002. Hyperplastic conotruncal endocardial cushions and transposition of great arteries in perlecan-null mice. *Circ. Res.* 91:158–164.
- Goyal, A., N. Pal, M. Concannon, M. Paul, M. Doran, C. Poluzzi, et al. 2011. Endorepellin, the angiostatic module of perlecan, interacts with both the alpha2beta1 integrin and vascular endothelial growth factor receptor 2 (VEGFR2): a dual receptor antagonism. *J. Biol. Chem.* 286:25947–25962.
- Hozumi, K., N. Suzuki, P. K. Nielsen, M. Nomizu, and Y. Yamada. 2006. Laminin alpha1 chain LG4 module promotes cell attachment through syndecans and cell spreading through integrin alpha2beta1. *J. Biol. Chem.* 281:32929–32940.
- Hummel, S., A. Osanger, T. M. Bajari, M. Balasubramani, W. Halfter, J. Nimpf, et al. 2004. Extracellular matrices of the avian ovarian follicle. Molecular characterization of chicken perlecan. *J. Biol. Chem.* 279:23486–23494.
- Iesaki, T., S. A. Gupte, P. M. Kaminski, and M. S. Wolin. 1999. Inhibition of guanylate cyclase stimulation by NO and bovine arterial relaxation to peroxynitrite and H₂O₂. *Am. J. Physiol.* 277:H978–H985.
- Inomata, T., N. Ebihara, T. Funaki, A. Matsuda, Y. Watanabe, L. Ning, et al. 2012. Perlecan-deficient mutation impairs corneal epithelial structure. *Invest. Ophthalmol. Vis. Sci.* 53:1277–1284.
- Iozzo, R. V. 2005. Basement membrane proteoglycans: from cellar to ceiling. *Nat. Rev. Mol. Cell Biol.* 6:646–656.
- Iozzo, R. V., and J. D. San Antonio. 2001. Heparan sulfate proteoglycans: heavy hitters in the angiogenesis arena. *J. Clin. Invest.* 108:349–355.

- Ishijima, M., N. Suzuki, K. Hozumi, T. Matsunobu, K. Kosaki, H. Kaneko, et al. 2012. Perlecan modulates VEGF signaling and is essential for vascularization in endochondral bone formation. *Matrix Biol.* 31:234–245.
- Jiang, X., and J. R. Couchman. 2003. Perlecan and tumor angiogenesis. *J. Histochem. Cytochem.* 51:1393–1410.
- Kaneko, H., M. Ishijima, I. Futami, N. Tomikawa-Ichikawa, K. Kosaki, R. Sadatsuki, et al. 2013. Synovial perlecan is required for osteophyte formation in knee osteoarthritis. *Matrix Biol.* 32:178–187.
- Kerever, A., J. Schnack, D. Vellinga, N. Ichikawa, C. Moon, E. Arikawa-Hirasawa, et al. 2007. Novel extracellular matrix structures in the neural stem cell niche capture the neurogenic factor fibroblast growth factor 2 from the extracellular milieu. *Stem Cells* 25:2146–2157.
- Laufs, U., V. La Fata, J. Plutzky, and J. K. Liao. 1998. Upregulation of endothelial nitric oxide synthase by HMG CoA reductase inhibitors. *Circulation* 97:1129–1135.
- McQuillan, L. P., G. K. Leung, P. A. Marsden, S. K. Kostyk, and S. Kourembanas. 1994. Hypoxia inhibits expression of eNOS via transcriptional and posttranscriptional mechanisms. *Am. J. Physiol.* 267:H1921–H1927.
- Nicole, S., C. S. Davoine, H. Topaloglu, L. Cattolico, D. Barral, P. Beighton, et al. 2000. Perlecan, the major proteoglycan of basement membranes, is altered in patients with Schwartz-Jampel syndrome (chondrodystrophic myotonia). *Nat. Genet.* 26:480–483.
- Nishida, K., D. G. Harrison, J. P. Navas, A. A. Fisher, S. P. Dockery, M. Uematsu, et al. 1992. Molecular cloning and characterization of the constitutive bovine aortic endothelial cell nitric oxide synthase. *J. Clin. Invest.* 90:2092–2096.
- Noonan, D. M., A. Fulle, P. Valente, S. Cai, E. Horigan, M. Sasaki, et al. 1991. The complete sequence of perlecan, a basement membrane heparan sulfate proteoglycan, reveals extensive similarity with laminin A chain, low density lipoprotein-receptor, and the neural cell adhesion molecule. *J. Biol. Chem.* 266:22939–22947.
- Papapetropoulos, A., R. D. Rudic, and W. C. Sessa. 1999. Molecular control of nitric oxide synthases in the cardiovascular system. *Cardiovasc. Res.* 43:509–520.
- Pillarsetti, S. 2000. Lipoprotein modulation of subendothelial heparan sulfate proteoglycans (perlecan) and atherogenicity. *Trends Cardiovasc. Med.* 10:60–65.
- Segev, A., N. Nili, and B. H. Strauss. 2004. The role of perlecan in arterial injury and angiogenesis. *Cardiovasc. Res.* 63:603–610.
- Sessa, W. C., K. Pritchard, N. Seyedi, J. Wang, and T. H. Hintze. 1994. Chronic exercise in dogs increases coronary vascular nitric oxide production and endothelial cell nitric oxide synthase gene expression. *Circ. Res.* 74:349–353.
- Stum, M., C. S. Davoine, S. Vicart, L. Guillot-Noel, H. Topaloglu, F. J. Carod-Artal, et al. 2006. Spectrum of HSPG2 (Perlecan) mutations in patients with Schwartz-Jampel syndrome. *Hum. Mutat.* 27:1082–1091.
- Sumiyoshi, K., H. Mokuno, T. Iesaki, K. Shimada, T. Miyazaki, A. Kume, et al. 2008. Deletion of the Fc receptors gamma chain preserves endothelial function affected by hypercholesterolaemia in mice fed on a high-fat diet. *Cardiovasc. Res.* 80:463–470.
- Tran-Lundmark, K., P. K. Tran, G. Paulsson-Berne, V. Friden, R. Soininen, K. Tryggvason, et al. 2008. Heparan sulfate in perlecan promotes mouse atherosclerosis: roles in lipid permeability, lipid retention, and smooth muscle cell proliferation. *Circ. Res.* 103:43–52.
- Tsumaki, N., K. Tanaka, E. Arikawa-Hirasawa, T. Nakase, T. Kimura, J. T. Thomas, et al. 1999. Role of CDMP-1 in skeletal morphogenesis: promotion of mesenchymal cell recruitment and chondrocyte differentiation. *J. Cell Biol.* 144:161–173.
- Vanhoutte, P. M. 2009. Endothelial dysfunction: the first step toward coronary arteriosclerosis. *Circ. J.* 73:595–601.
- Vikramadithyan, R. K., Y. Kako, G. Chen, Y. Hu, E. Arikawa-Hirasawa, Y. Yamada, et al. 2004. Atherosclerosis in perlecan heterozygous mice. *J. Lipid Res.* 45:1806–1812.
- Xu, Z., N. Ichikawa, K. Kosaki, Y. Yamada, T. Sasaki, L. Y. Sakai, et al. 2010. Perlecan deficiency causes muscle hypertrophy, a decrease in myostatin expression, and changes in muscle fiber composition. *Matrix Biol.* 29:461–470.
- Zembowicz, A., J. L. Tang, and K. K. Wu. 1995. Transcriptional induction of endothelial nitric oxide synthase type III by lysophosphatidylcholine. *J. Biol. Chem.* 270:17006–17010.
- Zoeller, J. J., J. M. Whitelock, and R. V. Iozzo. 2009. Perlecan regulates developmental angiogenesis by modulating the VEGF-VEGFR2 axis. *Matrix Biol.* 28:284–291.



Congenital myasthenic syndrome in Japan: Ethnically unique mutations in muscle nicotinic acetylcholine receptor subunits

Yoshiteru Azuma^{a,b}, Tomohiko Nakata^{a,b}, Motoki Tanaka^c, Xin-Ming Shen^d, Mikako Ito^a, Satoshi Iwata^a, Tatsuya Okuno^a, Yoshiko Nomura^e, Naoki Ando^f, Keiko Ishigaki^g, Bisei Ohkawara^a, Akio Masuda^a, Jun Natsume^b, Seiji Kojima^b, Masahiro Sokabe^c, Kinji Ohno^{a,*}

^a Division of Neurogenetics, Center for Neurological Diseases and Cancer, Nagoya University Graduate School of Medicine, Nagoya, Japan

^b Department of Pediatrics, Nagoya University Graduate School of Medicine, Nagoya, Japan

^c Department of Physiology, Nagoya University Graduate School of Medicine, Nagoya, Japan

^d Department of Neurology, Mayo Clinic, Rochester, MN, USA

^e Segawa Neurological Clinic for Children, Tokyo, Japan

^f Department of Pediatrics, Nagoya City University Graduate School of Medicine, Nagoya, Japan

^g Department of Pediatrics, Tokyo Women's Medical University, Tokyo, Japan

Received 29 May 2014; received in revised form 9 August 2014; accepted 3 September 2014

Abstract

Congenital myasthenic syndromes (CMS) are caused by mutations in genes expressed at the neuromuscular junction. Most CMS patients have been reported in Western and Middle Eastern countries, and only four patients with *COLQ* mutations have been reported in Japan. We here report six mutations in acetylcholine receptor (AChR) subunit genes in five Japanese patients. Five mutations are novel, and one mutation is shared with a European American patient but with a different haplotype. Among the observed mutations, p.Thr284Pro (p.Thr264Pro according to the legacy annotation) in the epsilon subunit causes a slow-channel CMS. Five other mutations in the delta and epsilon subunits are splice site, frameshift, null, or missense mutations causing endplate AChR deficiency. We also found a heteroallelic p.Met465Thr in the beta subunit in another patient. p.Met465Thr, however, was likely to be polymorphism, because single channel recordings showed mild shortening of channel openings without affecting cell surface expression of AChR, and the minor allelic frequency of p.Met465Thr was 5.1% in the Japanese population. Lack of shared mutant alleles between the Japanese and the other patients suggests that most mutations described here are ethnically unique or *de novo* in each family. © 2014 Elsevier B.V. All rights reserved.

Keywords: Congenital myasthenic syndromes; Acetylcholine receptor; Slow channel syndrome; Fast channel syndrome; Endplate acetylcholine receptor deficiency

1. Introduction

Acetylcholine released from the nerve terminal binds to muscle nicotinic acetylcholine receptor (AChR) at the motor endplate. AChR is clustered at the neuromuscular junction (NMJ) by binding to rapsyn with a stoichiometry of rapsyn to AChR of 1:1 to 2:1 [1]. AChR clustering is mediated by neural agrin that is released from the nerve terminal [2]. In early embryonic development, AChR clustering is also mediated by Wnt ligands [3,4]. Embryonic AChR is composed of α , β , δ , and γ subunits with a stoichiometry of $\alpha_2\beta\delta\gamma$. After birth, the ϵ

subunit is substituted for the γ subunit, generating $\alpha_2\beta\delta\epsilon$ -AChR.

Congenital myasthenic syndromes (CMS) are heterogeneous disorders caused by mutations in genes expressed at the NMJ [5]. They are characterized by fatigable muscle weakness, variable muscle atrophy, and sometimes dysmorphic features. CMS mutations have been reported in 19 genes, with most mutations in *CHRNA1*, *CHRN1*, *CHNRD*, and *CHNRE* encoding the AChR α , β , δ , and ϵ subunits, respectively. These mutations fall into three subsets: i) slow-channel CMS (SCCMS), in which the open time of AChR is abnormally prolonged; ii) fast-channel CMS (FCCMS), in which the open time of AChR is abnormally brief; and iii) endplate AChR deficiency. SCCMS is caused by a gain-of-function mutation and is dominantly inherited with variable penetrance [6]. In contrast, FCCMS and endplate AChR deficiency are caused by loss-of-function mutations on both alleles, and are recessively

* Corresponding author. Division of Neurogenetics, Center for Neurological Disease and Cancer, Nagoya University Graduate School of Medicine, 65 Tsurumai, Showa-ku, Nagoya 466-8550, Japan. Tel.: +81 52 744 2446; fax: +81 52 744 2449.

E-mail address: ohnok@med.nagoya-u.ac.jp (K. Ohno).

<http://dx.doi.org/10.1016/j.nmd.2014.09.002>

0960-8966/© 2014 Elsevier B.V. All rights reserved.

inherited. Low-expressor mutations of the AChR ϵ subunit are partly compensated for by expression of the embryonic AChR γ subunit, whereas the other AChR subunits have no substituting subunits. Accordingly, null and frameshift mutations are frequently detected in *CHRNE*, but not in the other subunit genes.

More than 500 patients with CMS have been reported in Western and Middle Eastern countries, whereas only four Japanese CMS patients carrying five mutations in *COLQ* encoding collagen Q that anchors acetylcholinesterase (AChE) at the NMJ have been reported by us [7,8]. Among the more than 450 CMS mutations in 19 disease genes registered in the Human Gene Mutation Database (<http://www.hgmd.org>), two likely have founder effects: p.Asn88Lys in *RAPSN* [9–11] and c.1124_1127dupTGCC in *DOK7* [12], whereas the others are private mutations occurring in a single or a small number of unrelated families. We here report five Japanese CMS patients with six mutations in the AChR subunit genes. We show that all the ten mutations in *COLQ*, *CHRND*, and *CHRNE* in Japanese patients are ethnically unique, which indicates that most CMS mutations arose *de novo* in recent human history or in each family.

2. Materials and methods

2.1. Ethical approval

All the human studies were approved by the institutional review boards of Nagoya University Graduate School of Medicine, Mayo Clinic, Segawa Neurological Clinic for Children, Nagoya City University, and Tokyo Women's Medical University. Appropriate written informed consent was obtained from all the patients and family members.

2.2. Mutation analysis and splicing analysis

Genomic DNA was isolated from peripheral blood with QIAamp Blood Kit (QIAGEN). We directly sequenced all exons with their flanking noncoding regions of *CHRNE*, *CHRNA1*, *CHRNB1*, and *CHRND* in this order with CEQ 8000 (Beckman Coulter). To look for large-scale DNA rearrangements in patient (Pt.) 4, we performed mate-pair sequencing of the whole genome using SOLiD4 (Life Technologies). The mate-pair library was made to span ~2 kb genomic segments according to the manufacturer's protocols. A total of 14.9 Gb of reads were mapped to human genome GRCh37/hg19 with the mapping efficiency of 89% using CLC Genomics Workbench (CLC Bio). All the reads mapped to *CHRNE* were visually scrutinized using Integrative Genome Browser (Broad Institute). Total RNA was isolated from biopsied muscle that was obtained for histopathological diagnostic purposes using RNeasy mini kit (QIAGEN). cDNA was synthesized with ReverTra Ace (Toyobo) and Oligo(dT) Primer (Life Technologies).

2.3. Expression of AChR subunit genes in HEK293 cells

Human α , β , δ , and ϵ subunit cDNAs were cloned into the CMV-based vector pRBG4 for expression in HEK293 cells [13]. The identified mutations were engineered into wild-type

AChR subunit cDNAs in pRBG4 using the QuikChange site-directed mutagenesis kit (Stratagene). Presence of each mutation and absence of unwanted artifacts were confirmed by sequencing the entire inserts. HEK293 cells were transfected with pRBG4- α , - β , - δ , - ϵ , and pcDNA3.1-EGFP at a ratio of 2:1:1:1:1 using FuGENE 6 transfection reagent (Promega). After 48 hrs, cells were incubated with α -bungarotoxin Alexa Flour 647 (Life Technologies) (1:200) in PBS for 1 hr. Signals were observed under an Olympus BX60 fluorescence microscope. The cells were trypsinized, washed with PBS, and resuspended in PBS. The total number of α -bungarotoxin-binding sites on the cell surface and EGFP was determined by the FACSCalibur system (BD Biosciences).

2.4. Single channel recordings

HEK293 cells were transfected with pRBG4- α , - β , - δ , and - ϵ , and pEGFP-N1 at a ratio of 2:1:1:1:1, using FuGENE 6. Recordings were obtained at 24 hrs after transfection in the cell-attached configuration at a membrane potential of -80 mV at 22 °C and with bath and pipette solutions containing (in mM): KCl, 142; NaCl, 5.4; CaCl₂, 1.8; MgCl₂, 1.7; HEPES, 10, pH 7.4. Single-channel currents were recorded using an Axopatch 200B amplifier (Axon Instruments) at a bandwidth of 50 kHz, digitized at 5- μ s intervals using Digidata 1322A (Axon Instruments) and recorded to a hard disk using the program Clampex 8.2 (Axon Instruments). Recordings obtained with ACh at 1 μ M or less were analyzed at a uniform bandwidth of 10–11.7 kHz with dead time of 15.3–17.9 μ s imposed. Recordings obtained with ACh at 10 μ M or more were analyzed with dead time at 25 μ s at 10 kHz with TAC software (Ver. x4.0.9, Bruxon). Dwell-time histograms were plotted on a logarithmic abscissa and fitted by the sum of exponentials by maximum likelihood, as previously reported [14].

3. Results

3.1. Clinical features

All Pts. had an abnormal decremental response to repetitive nerve stimulation, and no anti-AChR and anti-MuSK antibodies. Clinical features and repetitive nerve stimulation results are summarized in Table 1.

Pt. 1 (13 y.o., male) had eyelid ptosis since age six months and a positive edrophonium test. Clinical features were previously reported in a local journal [15]. Steroid pulse therapy at ages four and five years and thymectomy at age six years had no effect. Combined use of distigmine 3 mg/day and pyridostigmine 180 mg/day enabled him to sit in a chair without assistance at age 13 years. Biopsy of deltoid muscle at age eleven years showed marked AChR deficiency by fluorescent staining with α -bungarotoxin and simplified endplates by electron microscopy.

Pt. 2 (26 y.o., female) had nasal obstruction since birth and eyelid ptosis since age one month. She had a positive edrophonium test and was thought to have myasthenia gravis. Cholinesterase inhibitors were mildly effective. She has ophthalmoparesis, and is able to walk but is unable to run.

Table 1
Clinical features of six patients.

Pt.	Sex	Age	Onset	Consanguinity	Repetitive N. stimulation ^a	Drug ^b
1	M	13 y	6 m	–	Accessory N., 60%; Ulnar N., 53%	Distigmine 3 mg + pyridostigmine 180 mg, effective; 3,4-DAP 40 mg, mildly effective
2	F	26 y	1 m	+	Ulnar N., 80%	Pyridostigmine 150–180 mg, mildly effective
3	F	38 y	1 y	–	Ulnar N., 81%	Pyridostigmine 90–160 mg, moderately effective
4	F	6 y	2 y	–	Median N., 60%; Ulnar N., 68%	Pyridostigmine 90 mg + 3,4-DAP 30 mg, mildly effective; ephedrine 25 mg, effective
5	M	26 y	1 m	+	Ulnar N., 76%	Pyridostigmine 135 mg, moderately effective
6	M	11 y	Birth	–	Median N., 35%; Ulnar N., 31%	Prednisolone 35 mg <i>dieb. alt.</i> , effective

^a Repetitive N. stimulation, repetitive nerve stimulation at 2–3 Hz. Relative amplitudes of the 5th CMAP are indicated. ^b Simultaneous prescription is indicated by “+”.

Pt. 3 (38 y.o., female) had ptosis at age one year and was diagnosed to have myasthenia gravis at age seven years. Since then, she has been taking cholinesterase inhibitors and prednisolone, which seemed to help but could not climb steps after age 19 years.

Pt. 4 (6 y.o., female) walked alone at age 18 months, but since age two years she had repeated episodes of generalized muscle weakness that lasted about a week, especially when having a common cold. She could walk alone but was positive for a Gowers' sign. Cholinesterase inhibitors were moderately effective. Neurological examination of the mother detected no abnormality. The father was asymptomatic according to the mother, but was not examined by us. Clinical features were previously reported as patient 4 in a local journal [16].

Pt. 5 (26 y.o., male) had feeding difficulty at age one month and had eyelid ptosis since age five months. He has weak facial muscles and is unable to run. At age seven years, he had generalized muscle weakness during an upper respiratory infection. The edrophonium test was positive.

Pt. 6 (11 y.o., male) had repeated respiratory distress and respiratory infection during infancy. He walked alone at age one year, but was noticed to walk slowly at age five years with frequent falling episodes. Rest for a short time improved his walking, but there was no diurnal fluctuation of the symptoms. Intravenous administration of edrophonium chloride ameliorated walking difficulty, but long-acting cholinesterase inhibitors had no effect.

3.2. Mutation analysis

We directly sequenced AChR subunit genes in Pts. 1–6, and identified six mutations in *CHRND* and *CHRNE*, as well as a polymorphism in *CHRNBI* (Table 2). In this study, approved nucleotide and amino acid positions are used instead of the legacy annotation, in which nucleotide and amino acid positions start from the initiation sites of mature peptides.

Pt. 1 was compound heterozygous for c.1372-1G>A at the 3' end of intron 11 of *CHRND* and c.127C>T predicting p.Arg44Trp at the extracellular domain of the δ subunit (Fig. 1A). cDNA extracted from biopsied muscle revealed that a newly generated 'ag' dinucleotide that was one nucleotide downstream of the native 'ag' was used as a splice acceptor site (Fig. 1B), which predicted p.Glu458Argfs*20 in the long cytoplasmic loop of the δ subunit (Fig. 1A). Pt. 2 was homozygous for c.655_665del predicting p.Gly219Argfs*7 in the extracellular domain of the ϵ subunit (Fig. 1A). Pt. 3 was heterozygous for p.Tyr262Ter in the M1 transmembrane domain of the ϵ subunit (Fig. 1A). Pt. 4 was heterozygous for p.Thr284Pro in the M2 transmembrane domain of the ϵ subunit (Fig. 1A). Pt. 5 was homozygous for p.Leu304Arg in the short extracellular link between the M2 and M3 transmembrane domains of the ϵ subunit (Fig. 1A). Pt. 6 was heterozygous for p.Met465Thr close to the C-terminal end of the long cytoplasmic loop connecting the M3 and M4 transmembrane domains of AChR β subunit (Fig. 1A).

Table 2
Six mutations and one polymorphism identified in AChR subunit genes.

Pt.	Gene	Nucleotide change ^c	Amino-acid change ^c	Legacy annotation ^d	Phenotypic consequence
1	<i>CHRND</i>	c.1372-1G>A	δ p.Glu458Argfs*20	δ E437fs	AChR deficiency
	<i>CHRND</i>	c.127C>T	δ p.Arg44Trp	δ R23W	AChR deficiency
2 ^a	<i>CHRNE</i>	c.655_665del	ϵ p.Gly219Argfs*7	ϵ G199fs	AChR deficiency
3 ^b	<i>CHRNE</i>	c.786C>G	ϵ p.Tyr262Ter	ϵ Y242X	AChR deficiency
4	<i>CHRNE</i>	c.850A>C	ϵ p.Thr284Pro	ϵ T264P	SCCMS
5 ^a	<i>CHRNE</i>	c.911T>G	ϵ p.Leu304Arg	ϵ L284R	AChR deficiency
6	<i>CHRNBI</i>	c.1394T>C	ϵ p.Met465Thr	β M442T	~50% shortening of AChR openings

^a Patient is homozygous for the mutation.

^b A mutation on another allele remains unidentified.

^c Nucleotide and amino acid positions start from the translational start sites.

^d In legacy annotation, nucleotide and amino acid positions start from the initiation sites of mature peptides, which are 69 nt. (23 amino acids), 63 nt. (21 amino acids), and 60 nt. (20 amino acids) downstream of the translational start sites of *CHRNBI*, *CHRND*, and *CHRNE*, respectively.

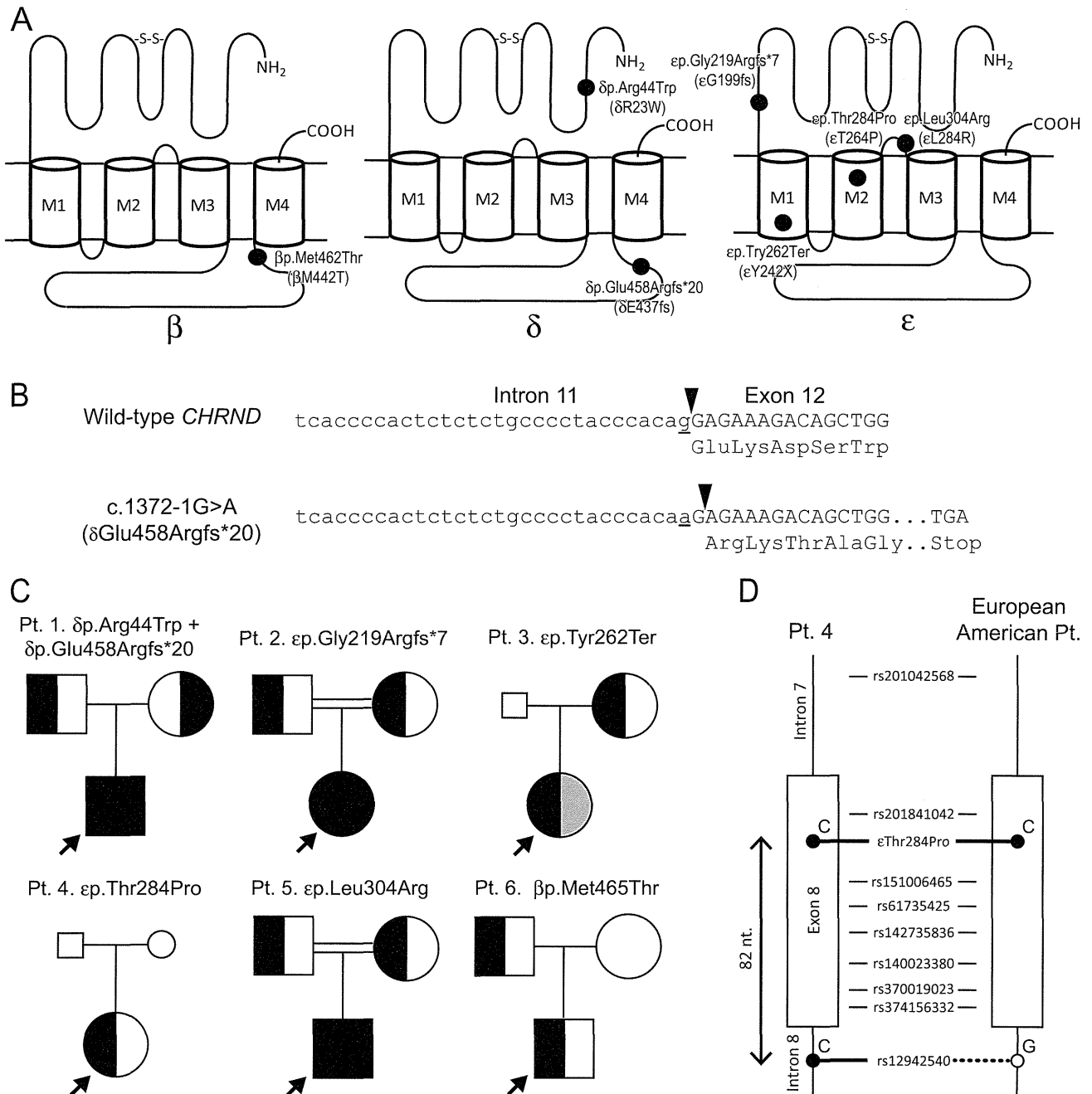


Fig. 1. Six mutations and a single polymorphism in AChR subunit genes identified in six CMS patients. (A) Positions of six mutations and a polymorphism. M1-M4, the first to fourth transmembrane domains. The M2 domains form a channel pore of AChR. (B) RT-PCR of biopsied muscle of Pt. 1 reveals that c.1372-1G>A (underlined) shifts a splice acceptor site (arrowheads) one nucleotide downstream, which predicts a shift in the reading frame (δp.Glu458Argfs*20). (C) Pedigree analyses of the mutations. Patients are indicated by arrows. Full and half shaded symbols represent homozygous and heterozygous mutations, respectively. Gray half shaded symbols represent that the individuals are predicted to carry a heterozygous mutation, the identity of which, however, has not been identified. Small symbols indicate that DNA is not available. (D) Haplotype analysis of ep.Thr284Pro in Pt. 4 and the previously reported European American Pt [7]. Both patients carry discordant nucleotides at rs12942540, which is 82 nt. downstream of the mutation.

δp.Arg44Trp (rs55868108) in Pt. 1 was previously reported in one of five healthy controls, but its ethnic origin was not documented [17]. δp.Arg44Trp, however, is not observed in the 1000 genome project (<http://www.1000genomes.org/>) or in the

human gene variation database (HGVD), which collates SNPs in a large cohort of Japanese individuals (<http://www.genome.med.kyoto-u.ac.jp/SnpDB/>) [18]. As indicated below, functional analysis disclosed that δp.Arg44Trp

Table 3

Open intervals and bursts of wild-type and mutant AChR expressed on HEK cells.

	Open intervals		Bursts	
	Wild-type	β p.Met465Thr	Wild-type	β p.Met465Thr
τ_1 (ms)	0.037 ± 0.0033^a	0.022^b	0.036 ± 0.0017^c	0.039 ± 0.006^d
(a ₁)	(0.17 \pm 0.022)	(0.18)	(0.24 \pm 0.021)	(0.18 \pm 0.034)
τ_2 (ms)	0.31 ± 0.050	0.16 ± 0.017^e	0.47 ± 0.059	0.16 ± 0.037^f
(a ₂)	(0.27 \pm 0.038)	(0.23 \pm 0.031)	(0.21 \pm 0.027)	(0.23 \pm 0.010)
τ_3 (ms)	1.35 ± 0.051	0.98 ± 0.034	3.31 ± 0.12	1.93 ± 0.085
(a ₃)	(0.67 \pm 0.042)	(0.78 \pm 0.028)	(0.58 \pm 0.038)	(0.82 \pm 0.034)

Twenty-one wild-type and seven mutant patches were analyzed. Time constants, τ_n , and fractional areas, a_n, for each component are presented with mean \pm SEM. ACh concentration was 50–100 nM.

^{a-f} Not detected at 12, 6, 3, 5, 1, and 3 patches, respectively.

Final band widths were 11.7 and 10 kHz for wild-type and mutant AChRs, respectively.

significantly reduces cell surface expression of AChR and is unlikely to be polymorphism.

p.Met465Thr (rs201776800) in Pt. 6 was observed in eight alleles in eight Japanese individuals in the 1000 genome project with a minor allelic frequency (MAF) of 0.004, as well as in 119 alleles in a cohort of 1170 Japanese individuals in HGVD with a MAF of 0.051. Although p.Met465Thr was likely to be a polymorphism according to the high MAFs in the Japanese, we scrutinized functional consequences of p.Met465Thr in this study.

3.3. *ep.Gly219Argfs*7*, *ep.Tyr262Ter*, and *δ p.Glu458Argfs*20* are predicted to compromise AChR expression

Among the six mutations, *ep.Gly219Argfs*7* in Pt. 2 and *ep.Tyr262Ter* in Pt. 3 were predicted to produce truncated ϵ subunits. We previously reported that truncation mutations in the ϵ subunit lead to expression of the embryonic $\alpha_2\beta\delta\gamma$ -AChR at the patient's endplates and the patients have endplate AChR deficiency [19–21]. The ϵ mutations in Pts. 2 and 3 were thus predicted to cause AChR deficiency.

*δ p.Glu458Argfs*20* in Pt. 1 was predicted to generate a truncated δ subunit that cannot be incorporated into mature AChR. The phenotype of Pt. 1 is thus determined by *δ p.Arg44Trp* on the other allele, which causes AChR deficiency as indicated below.

3.4. *ep.Thr284Pro* is an established slow-channel mutation without shared haplotype with a European American patient

ep.Thr284Pro in the M2 domain of the ϵ subunit was identical to the first characterized slow-channel mutation reported in a patient of Swiss and Turkish descent [22]. We asked if the mutation in Pt. 4 derived from the same founder allele as the first reported patient. Therefore we sequenced exon 8 and its flanking intronic regions where nine SNPs were located (Fig. 1C). This revealed that the mutant allele in the Japanese patient had 'C', whereas the mutant allele in the European American patient had 'G' at rs12942540 in intron 8, which was located 82 nt. downstream of *ep.Thr284Pro*. Accordingly, *ep.Thr284Pro* in both patients is likely to have occurred independently in two ethnic groups.

3.5. *δ p.Arg44Trp* and *ep.Leu304Arg*, but not *β p.Met465Thr*, decrease cell surface expression of AChR in transfected HEK293 cells

We next analyzed the effects of AChR expression of the remaining three mutations of *δ p.Arg44Trp*, *ep.Leu304Arg* and *β p.Met465Thr*. We introduced wild-type or mutant α , β , δ , and ϵ subunit cDNAs along with EGFP cDNA into HEK293 cells (Fig. 2A), and measured cell surface expression of AChR detected by Alexa 647-labeled α -bungarotoxin using FACS. Expression of *β p.Met465Thr*-AChR was similar to that of wild-type AChR, whereas *δ p.Arg44Trp* and *ep.Leu304Arg* markedly attenuated the cell surface expression of AChR (Figs. 2B and C). Accordingly, *δ p.Arg44Trp* and *ep.Leu304Arg* cause endplate AChR deficiency.

3.6. *β p.Met465Thr* mildly shortens channel opening events, but not as much as the other established fast channel mutations

As *β p.Met465Thr*-AChR was efficiently expressed on HEK293 cells, we next recorded opening and closing of single AChR channels at limiting low concentrations of ACh by the patch clamp method (Fig. 3A). We found that the major burst duration (τ_3) was decreased from 3.31 ms to 1.93 ms (58.3%) in *β p.Met465Thr*-AChR (Table 3), while the conductance of *β p.Met465Thr*-AChR was normal. Distributions of opening probabilities of the clusters generated by 10 μ M or greater concentrations of ACh made single peaks for both wild-type and mutant AChRs. Thus, *β p.Met465Thr* mildly shortens the channel openings but does not cause a mode switching in the kinetics of the receptor activation, which is seen in other FCCMS mutations [23,24].

3.7. A recessive mutation on the other allele in Pt. 3 remains unidentified

Functional prediction and characterization of the six mutations indicated that *ep.Thr284Pro* in Pt. 4 was a dominant slow-channel mutation [22], whereas the other five mutations in Pts. 1, 2, 3, and 5 were recessive loss-of-function mutations. The mutations in Pts. 1, 2, and 5 were biallelic, whereas a mutation was detected only on a single allele in Pt. 3 (Fig. 1C).

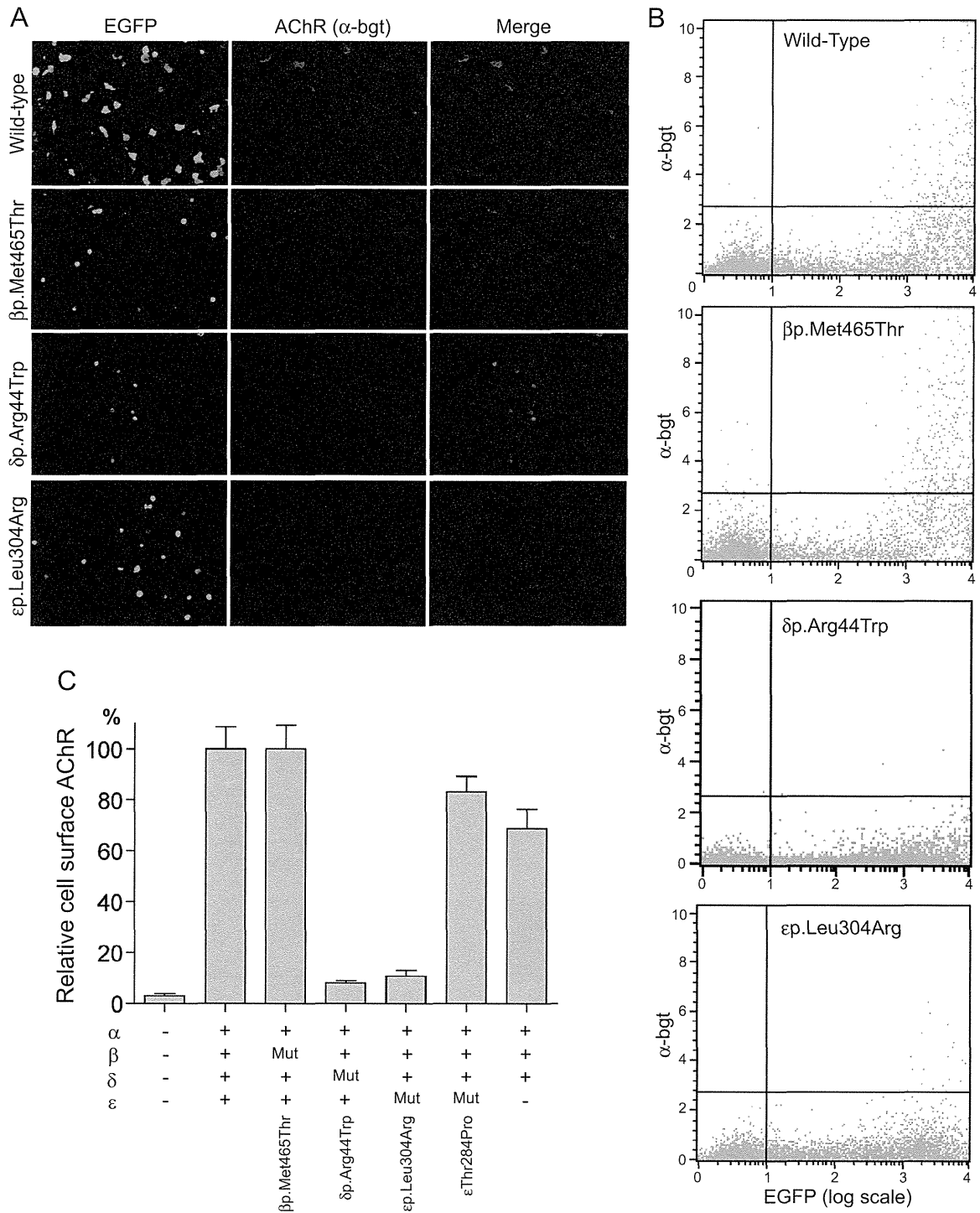


Fig. 2. Quantification of cell surface expression of wild-type and mutant AChRs on HEK293 cells. (A) HEK293 cells are transfected with wild-type or mutant AChR subunit cDNAs along with EGFP cDNA. Only transfected cells have EGFP signals and AChRs that are visualized with Alexa 647-labeled α -bungarotoxin (bgt). ep.Leu304Arg-AChR has less signals for AChRs compared to wild-type and β p.Met465Thr-AChRs. (B) Representative FACS profiles of EGFP and Alexa 647-labeled α -bgt. Both axes are shown in arbitrary units. The number of cells fractionated into the upper right quadrant is counted as AChR-positive cells. (C) Ratios of AChR-positive cells (the upper right quadrant) divided by EGFP-positive cells (the lower right quadrant). δ p.Arg44Trp and ep.Leu304Arg markedly decrease AChR expression, whereas β p.Met465Thr and ep.Thr284Pro have no effect on AChR expression. ϵ -deficient $\alpha_2\beta\delta_2$ -AChR are expressed at ~70% of wild-type, as we reported previously [21]. Mut, a mutant AChR subunit. Mean and SE are indicated ($n = 12$).

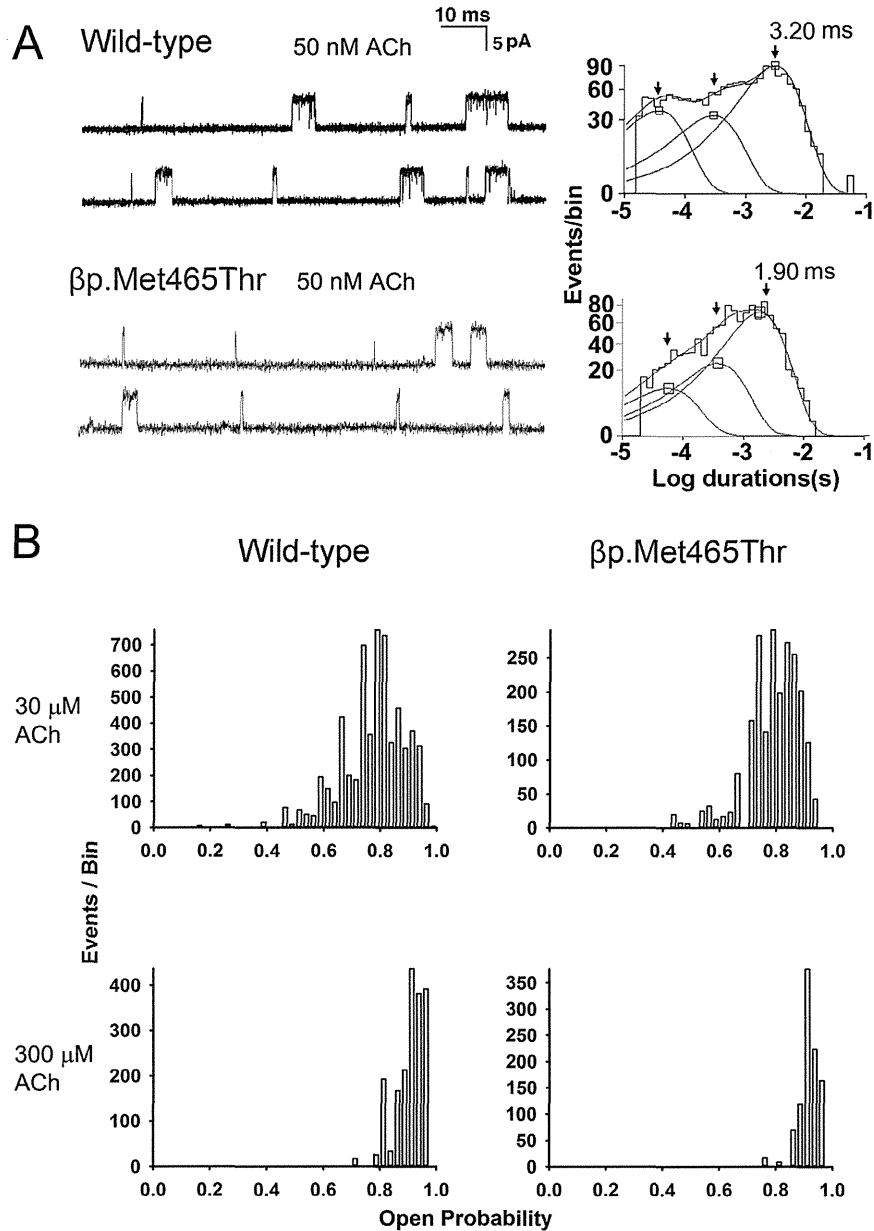


Fig. 3. Single channel currents of wild-type and mutant AChRs on HEK293 cells. (A) Left: Representative channel openings shown as upward deflections. Right: Burst duration histograms fitted to the sum of exponentials. Arrows indicate mean durations of dominant burst components. (B) Distribution of open probabilities from individual clusters obtained at the indicated ACh concentrations. Note that both wild-type and mutant AChRs make a single peak.

We scrutinized all exonic nucleotides in *CHRNE* in Pt. 3 by bidirectional sequencing, but detected none. We therefore hypothesized that a mutation on the other alleles was either a promoter mutation, a splice-site mutation disrupting a deep intronic splicing *cis*-element, or a large-scale DNA rearrangement. Sequencing of \sim 1 kb upstream of the translation initiation sites, however, revealed no mutation. We further analyzed genomic DNA by mate-pair sequencing of the whole genome. A total of 57 reads were mapped to *CHRNE*. Visual

inspection of these reads, however, failed to detect any large-scale DNA rearrangements or any mutations. A recessive mutation on the other allele in *CHRNE* in Pt. 3 thus remains unidentified. We also analyzed 18 other CMS-causing genes using the mate-pair sequencing data in Pt. 3. As the mate-pair sequencing was for detecting a large-scale DNA rearrangement, the 18 genes were covered by only 10,116 reads. Although the coverage was not high enough for detecting SNVs, no candidate mutations were detected in Pt. 3.

Table 4

Fifteen previously reported FCCMS mutations and the currently analyzed β p.Met462Thr polymorphism.

Mutation	Burst duration (ms)			Expression (%)	Domain	Reference
	Wild-type	Mutant	Ratio			
α p.Val152Leu (α V132L)	3.31	0.50	0.151	135	Extracellular domain of α	[25]
α p.Val208Met (α V188M)	3.31	0.68	0.205	90	Extracellular domain of α	[26]
α p.Phe276Leu (α F256L)	3.62	0.30	0.083	102	M2 domain of α	[27]
α p.Val305Ile (α V285I)	2.99	0.34	0.114	116	M3 domain of α	[28]
δ p.Leu63Pro (δ L42P)	3.31	0.18	0.054	37	Extracellular domain of δ	[14]
δ p.Glu80Lys (δ E59K)	5.06	2.75	0.543	62	Extracellular domain of δ	[29]
δ p.Pro271Gln (δ P250Q)	3.31	1.54	0.465	60	M1 domain of δ	[30]
ep.Thr58Lys (ϵ T38K)	5.86	0.06	0.010	78	Extracellular domain of ϵ	[31]
ep.Trp75Arg (ϵ W55R)	3.31	0.37	0.112	86	Extracellular domain of ϵ	[32]
ep.Pro141Leu (ϵ P121L)	2.99	0.45	0.151	102	Extracellular domain of ϵ	[13]
ep.Asp195Asn (ϵ D175N)	2.13	0.49	0.230	117 ^b	Extracellular domain of ϵ	[33]
ep.Asn202Tyr (ϵ N182Y)	2.13	0.65	0.305	117 ^b	Extracellular domain of ϵ	[33]
ep.Ser433_Glu438dup (ϵ I254ins18)	2.80	1.01	0.361	47	Long cytoplasmic loop of ϵ	[23]
ep.Ala431Pro (ϵ A411P)	n.a. ^a	n.a. ^a	n.a. ^a	31	Long cytoplasmic loop of ϵ	[24]
ep.Asn456del (ϵ N436del)	3.31	1.24	0.375	51	Long cytoplasmic loop of ϵ	[34]
β p.Met462Thr (β M442T)	3.31	1.93	0.583	99	Long cytoplasmic loop of β	Current study

A major component of burst durations of wild-type and mutant AChRs expressed in HEK293 cells is indicated. Cell surface expression in HEK293 cells is normalized to that of wild-type. Channel openings are elicited by 50–100 nM ACh. Mutations in parentheses are legacy annotations used in original reports.

^a Detailed ion channel kinetics are analyzed using a hidden Markov model, but burst durations are not indicated.

^b Cell surface expression of recombinant AChR is not indicated, and the expression ratio is calculated from α -bungarotoxin binding sites of control and patient endplates.

4. Discussion

We identified six mutations in AChR subunit genes in five Japanese patients with CMS. We initially assumed that β p.Met465Thr in Pt. 6 was a mild fast-channel mutation. However, expansion of the SNP database later disclosed that β p.Met465Thr is a polymorphism that is frequently observed in the Japanese population. Fifteen previously reported FCCMS mutations shorten burst durations to $22.6 \pm 16.1\%$ of wild-type (mean and SD; range 1.0%–54.3%) (Table 4). A FCCMS mutation, δ p.Glu80Lys (δ E59K), decreases burst durations to 54.3% of wild-type [29], which is similar to 58.3% observed in the current β p.Met465Thr polymorphism. However, in contrast to β p.Met465Thr, δ p.Glu80Lys reduces cell surface expression of AChR to 62% of wild-type [29]. Similarly, δ p.Pro271Gln (δ P250Q) mildly reduces burst durations to 46.5% of wild-type, but again, unlike β p.Met465Thr, this mutation reduces cell surface expression of AChR to 60% of wild-type [30]. A plot of normalized burst durations and normalized cell surface expressions suggests that a mean burst duration of less than $\sim 30\%$ causes FCCMS even when it does not affect the cell surface expression of AChR (Fig. 4). In contrast, a mean burst duration of between $\sim 30\%$ and $\sim 60\%$ causes FCCMS when the mutation reduces the cell surface expression of AChR to $\sim 60\%$ or less (Fig. 4). However, as no individual is homozygous for β p.Met465Thr or carries a null mutation on the other allele, pathogenicity of β p.Met465Thr in the absence of a normal *CHRNA2* on the other allele still remains unknown.

δ p.Arg44Trp is close to the N-terminal end of the extracellular region (Fig. 5). We previously reported that a similar ep.Arg40Trp also causes AChR deficiency [35]. The specific function of this region, however, is not well dissected. ep.Leu304Arg is in the short extracellular link between the M2

and M3 transmembrane domains (Fig. 5). The functions of this link are not well characterized. In this link, only α p.Ser289Ile (α S269I) is reported in SCCMS [38]. β p.Met465Thr is located close to the C-terminal end of the long cytoplasmic loop that links the M3 and M4 transmembrane domains (Fig. 5). Interestingly, three FCCMS mutations in the long cytoplasmic loop are clustered close to the C-terminal end of the ϵ subunit [23,24,34,36,37], and similarly destabilize the channel open state. Two FCCMS mutations in this region, ep.Ser433_Glu438dup (ϵ I254ins18) [23] and ep.Ala431Pro (ϵ A411P) [24], disrupt the fidelity of gating and result in unstable channel kinetics. In addition, another FCCMS

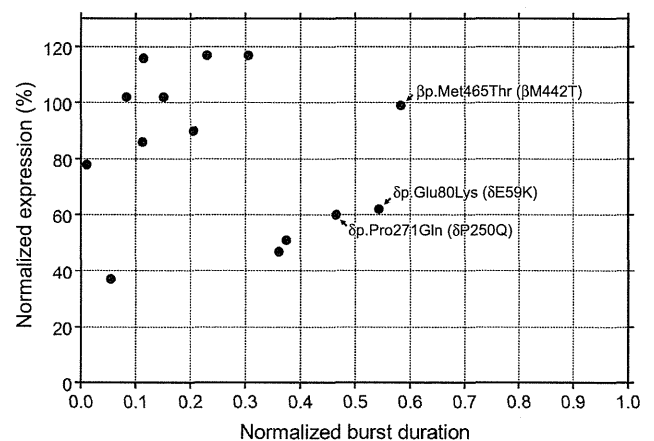


Fig. 4. Normalized burst durations and normalized cell surface expressions of previously reported FCCMS mutations and the currently analyzed β p.Met462Thr polymorphism shown in Table 4. Arrows point to mutations and a polymorphism that are addressed in the discussion.

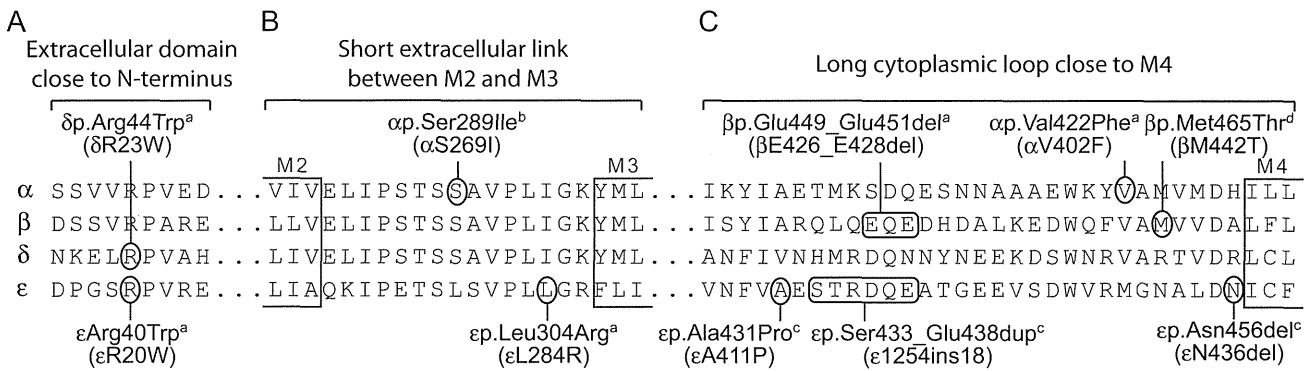


Fig. 5. Positions of the currently identified δ p.Arg44Trp, ep.Leu304Arg and β p.Met465Thr, as well as previously reported CMS mutations. Mutations in the extracellular domain close the N-terminal end (A), the short extracellular link between the M2 and M3 transmembrane domains (B), and the long cytoplasmic loop close to the M4 transmembrane domain (C) are indicated. ^a δ p.Arg44Trp (current report), ep.Arg40Trp [35], β p.Glu449_Glu451 del [36], and α p.Val422Phe [37] cause AChR deficiency (AChR def.). ^b α p.Ser289Ile [38] causes SCCMS. ^cep.Ala431Pro [24], ϵ p.Ser433_Glu438dup [23], and ep.Asn456del [34] cause FCCMS. ^d β p.Met465Thr is a currently analyzed polymorphism that shortens channel opening events. Mutations in parentheses are legacy annotations used in the original reports.

mutation in this region, ep.Asn456del (ϵ N436del), destabilizes the diliganded receptor [34]. The C-terminal region of the long cytoplasmic loop of the ϵ subunit is thus likely to be crucial for stabilizing the open channel. In contrast to the three FCCMS mutations in the C-terminal end, however, β p.Met465Thr mildly shortens channel opening events and has no effect on the fidelity of channel gating, which may represent subunit-specificity and/or position-specificity of the amino acid substitutions.

Excluding δ p.Arg44Trp that was previously reported in a healthy subject of unknown ethnicity [17], five of the six mutations in the AChR subunit genes in the current study and the five previously identified *COLQ* mutations [8] are unique to Japanese people. This is in contrast to some CMS mutations that are observed in unrelated families in Western and Middle Eastern countries. Especially, founder effects are implicated in two mutations: p.Asn88Lys in *RAPSN* [9–11] and c.1124_1127dupTGCC in *DOK7* [12]. CMS mutations are all recessively inherited except for those causing SCCMS. As heterozygous carriers of recessive CMS mutations exhibit no clinical phenotypes even by detailed electrophysiological studies, an asymptomatic carrier of a recessive CMS mutation has no disadvantage in transmitting the mutant allele to offspring. Lack of founder effects between the Japanese patients and patients of other nationalities thus suggest that most but not all CMS mutations arose *de novo* in a recent human history or in each family.

Acknowledgments

This study was supported by Grants-in-Aid from the MEXT and MHLW of Japan to KO. We would like to thank Dr. Andrew G. Engel for critical and constructive discussion on this project.

References

- [1] Borges LS, Yechikhov S, Lee YI, et al. Identification of a motif in the acetylcholine receptor beta subunit whose phosphorylation regulates

- rapsyn association and postsynaptic receptor localization. *J Neurosci* 2008;28:11468–76.
- [2] Bezakova G, Ruegg MA. New insights into the roles of agrin. *Nat Rev Mol Cell Biol* 2003;4:295–308.
- [3] Budnik V, Salinas PC. Wnt signaling during synaptic development and plasticity. *Curr Opin Neurobiol* 2011;21:151–9.
- [4] Korkut C, Budnik V. WNTs tune up the neuromuscular junction. *Nat Rev Neurosci* 2009;10:627–34.
- [5] Ohno K, Ito M, Engel AG. Congenital myasthenic syndromes – molecular bases of congenital defects of proteins at the neuromuscular junction. In: Zaher A, editor. *Neuromuscul. Disord. Rijeka: InTech; 2012. p. 175–200.*
- [6] Croxen R, Hatton C, Shelley C, et al. Recessive inheritance and variable penetrance of slow-channel congenital myasthenic syndromes. *Neurology* 2002;59:162–8.
- [7] Ohno K, Engel AG, Brengman JM, et al. The spectrum of mutations causing endplate acetylcholinesterase deficiency. *Ann Neurol* 2000;47:162–70.
- [8] Nakata T, Ito M, Azuma Y, et al. Mutations in the C-terminal domain of ColQ in endplate acetylcholinesterase deficiency compromise ColQ-MuSK interaction. *Hum Mutat* 2013;34:997–1004.
- [9] Ohno K, Engel AG. Lack of founder haplotype for the rapsyn N88K mutation: N88K is an ancient founder mutation or arises from multiple founders. *J Med Genet* 2004;41:e8.
- [10] Muller JS, Abicht A, Burke G, et al. The congenital myasthenic syndrome mutation *RAPSN* N88K derives from an ancient Indo-European founder. *J Med Genet* 2004;41:e104.
- [11] Dunne V, Maselli RA. Common founder effect of rapsyn N88K studied using intragenic markers. *J Hum Genet* 2004;49:366–9.
- [12] Ben Ammar A, Petit F, Alexandri N, et al. Phenotype genotype analysis in 15 patients presenting a congenital myasthenic syndrome due to mutations in *DOK7*. *J Neurol* 2010;257:754–66.
- [13] Ohno K, Wang HL, Milone M, et al. Congenital myasthenic syndrome caused by decreased agonist binding affinity due to a mutation in the acetylcholine receptor epsilon subunit. *Neuron* 1996;17:157–70.
- [14] Shen XM, Fukuda T, Ohno K, Sine SM, Engel AG. Congenital myasthenia-related AChR delta subunit mutation interferes with intersubunit communication essential for channel gating. *J Clin Invest* 2008;118:1867–76.
- [15] Ishigaki K, Murakami T, Ito Y, et al. [Treatment approach to congenital myasthenic syndrome in a patient with acetylcholine receptor deficiency]. *No to Hattatsu* 2009;41:37–42.
- [16] Irahara K, Komaki H, Honda R, et al. [Clinical features of congenital myasthenic syndrome in Japan]. *No to Hattatsu* 2012;44:450–4.
- [17] Denning L, Anderson JA, Davis R, Gregg JP, Kuzdenyi J, Maselli RA. High throughput genetic analysis of congenital myasthenic syndromes using resequencing microarrays. *PLoS ONE* 2007;2:e918.

- [18] Narahara M, Higasa K, Nakamura S, et al. Large-scale East-Asian eQTL mapping reveals novel candidate genes for LD mapping and the genomic landscape of transcriptional effects of sequence variants. *PLoS ONE* 2014;9:e100924.
- [19] Engel AG, Ohno K, Bouzat C, Sine SM, Griggs RC. End-plate acetylcholine receptor deficiency due to nonsense mutations in the epsilon subunit. *Ann Neurol* 1996;40:810–17.
- [20] Engel AG, Ohno K, Milone M, et al. New mutations in acetylcholine receptor epsilon subunit genes reveal heterogeneity in the slow-channel congenital myasthenic syndrome. *Hum Mol Genet* 1996;5:1217–27.
- [21] Ohno K, Quiram PA, Milone M, et al. Congenital myasthenic syndromes due to heteroallelic nonsense/missense mutations in the acetylcholine receptor epsilon subunit gene: identification and functional characterization of six new mutations. *Hum Mol Genet* 1997;6:753–66.
- [22] Ohno K, Hutchinson DO, Milone M, et al. Congenital myasthenic syndrome caused by prolonged acetylcholine receptor channel openings due to a mutation in the M2 domain of the epsilon subunit. *Proc Natl Acad Sci U S A* 1995;92:758–62.
- [23] Milone M, Wang H-L, Ohno K, et al. Mode switching kinetics produced by a naturally occurring mutation in the cytoplasmic loop of the human acetylcholine receptor epsilon subunit. *Neuron* 1998;20:575–88.
- [24] Wang H-L, Ohno K, Milone M, et al. Fundamental gating mechanism of nicotinic receptor channel revealed by mutation causing a congenital myasthenic syndrome. *J Gen Physiol* 2000;116:449–62.
- [25] Shen X-M, Ohno K, Tsujino A, et al. Mutation causing severe myasthenia reveals functional asymmetry of AChR signature cysteine loops in agonist binding and gating. *J Clin Invest* 2003;111:497–505.
- [26] Shen XM, Brengman JM, Sine SM, Engel AG. Myasthenic syndrome AChRalpha C-loop mutant disrupts initiation of channel gating. *J Clin Invest* 2012;122:2613–21.
- [27] Webster R, Brydson M, Croxen R, Newsom-Davis J, Vincent A, Beeson D. Mutation in the AChR ion channel gate underlies a fast channel congenital myasthenic syndrome. *Neurology* 2004;62:1090–6.
- [28] Wang H-L, Milone M, Ohno K, et al. Acetylcholine receptor M3 domain: stereochemical and volume contributions to channel gating. *Nat Neurosci* 1999;2:226–33.
- [29] Brownlow S, Webster R, Croxen R, et al. Acetylcholine receptor d subunit mutations underlie a fast-channel myasthenic syndrome and arthrogyriposis multiplex congenita. *J Clin Invest* 2001;108:125–30.
- [30] Shen XM, Ohno K, Fukudome T, et al. Congenital myasthenic syndrome caused by low-expressor fast-channel AChR delta subunit mutation. *Neurology* 2002;59:1881–8.
- [31] Webster R, Liu WW, Chaouch A, Lochmuller H, Beeson D. Fast-channel congenital myasthenic syndrome with a novel acetylcholine receptor mutation at the alpha-epsilon subunit interface. *Neuromuscul Disord* 2014;24:143–7.
- [32] Shen XM, Brengman JM, Edvardson S, Sine SM, Engel AG. Highly fatal fast-channel syndrome caused by AChR epsilon subunit mutation at the agonist binding site. *Neurology* 2012;79:449–54.
- [33] Sine SM, Shen X-M, Wang H-L, et al. Naturally occurring mutations at the acetylcholine receptor binding site independently alter ACh binding and channel gating. *J Gen Physiol* 2002;120:483–96.
- [34] Shen XM, Ohno K, Sine SM, Engel AG. Subunit-specific contribution to agonist binding and channel gating revealed by inherited mutation in muscle acetylcholine receptor M3-M4 linker. *Brain* 2005;128:345–55.
- [35] Shen X-M, Ohno K, Milone M, Brengman JM, Spilsbury P, Engel AG. Low-affinity fast-channel syndrome. *Neurology* 2001;56(Suppl. 3):A60. (abstract).
- [36] Quiram PA, Ohno K, Milone M, et al. Mutation causing congenital myasthenia reveals acetylcholine receptor beta/delta subunit interaction essential for assembly. *J Clin Invest* 1999;104:1403–10.
- [37] Milone M, Shen X-M, Ohno K, et al. Unusual congenital myasthenic syndrome with endplate AChR deficiency caused by alpha subunit mutations and a remitting-relapsing clinical course. *Neurology* 1999;51(Suppl. 2):A185. (abstract).
- [38] Croxen R, Newland C, Beeson D, et al. Mutations in different functional domains of the human muscle acetylcholine receptor alpha subunit in patients with the slow-channel congenital myasthenic syndrome. *Hum Mol Genet* 1997;6:767–74.

Original Investigation

Impaired Synaptic Development, Maintenance, and Neuromuscular Transmission in LRP4-Related Myasthenia

Duygu Selcen, MD; Bisei Ohkawara, PhD; Xin-Ming Shen, PhD; Kathleen McEvoy, MD; Kinji Ohno, MD, PhD; Andrew G. Engel, MD

IMPORTANCE Congenital myasthenic syndromes (CMS) are heterogeneous disorders. Defining the phenotypic features, genetic basis, and pathomechanisms of a CMS is relevant to prognosis, genetic counseling, and therapy.

OBJECTIVES To characterize clinical, structural, electrophysiologic, and genetic features of a CMS and to search for optimal therapy.

DESIGN, SETTINGS, AND PARTICIPANTS Two sisters with CMS affecting the limb-girdle muscles were investigated between 2012 and 2014 at an academic medical center by clinical observation, in vitro analysis of neuromuscular transmission, cytochemical and electron microscopy studies of the neuromuscular junction, exome sequencing, expression studies in HEK293 and COS7 cells, and for response to therapy, and they were compared with 15 historical control participants.

MAIN OUTCOMES AND MEASURES We identified the disease gene and mutation, confirmed pathogenicity of the mutation by expression studies, and instituted optimal pharmacotherapy.

RESULTS Quantitative analysis of single EP regions was done for all 15 control participants and microelectrode studies of neuromuscular transmission and α -bgt binding sites per EP was conducted for 13 control participants. Examination of the older sister's intercostal muscle end plates (EPs) showed them to be abnormally small, with attenuated reactivities for the acetylcholine receptor and acetylcholinesterase. Most EPs had poorly differentiated or degenerate junctional folds, and some appeared denuded of nerve terminals. The amplitude of the EP potential (EPP), the miniature EPP, and the quantal content of the EPP were all markedly reduced. Exome sequencing identified a novel homozygous p.Glu1233Ala mutation in low-density lipoprotein receptor-related protein 4 (LRP4), a coreceptor for agrin to activate muscle-specific tyrosine kinase (MuSK), which is required for EP development and maintenance. Expression studies indicate that the mutation compromises the ability of LRP4 to bind to, phosphorylate, and activate MuSK. Treatment with albuterol sulfate improved the patients' symptoms. A previously identified patient harboring 2 heterozygous mutations in LRP4 had structurally abnormal intercostal EPs but no identifiable defect of neuromuscular transmission at these EPs.

CONCLUSIONS AND RELEVANCE We identified a second CMS kinship harboring mutations in *LRP4*, identified the mechanisms that impair neuromuscular transmission, and mitigated the disease by appropriate therapy.

Author Affiliations: Department of Neurology, Mayo Clinic, Rochester, Minnesota (Selcen, Shen, McEvoy, Engel); Division of Neurogenetics, Center for Neurological Diseases and Cancer, Nagoya University Graduate School of Medicine, Nagoya, Japan (Ohkawara, Ohno).

Corresponding Author: Andrew G. Engel, MD, Department of Neurology, Mayo Clinic, 200 First St SW, Rochester, MN 55905 (age@mayo.edu).

JAMA Neurol. 2015;72(8):889-896. doi:10.1001/jamaneurol.2015.0853
Published online June 8, 2015.

The development and maintenance of the neuromuscular junction depends crucially on the agrin-MuSK-LRP4 signaling system. Low-density lipoprotein receptor-related protein 4 (LRP4) and muscle-specific tyrosine kinase (MuSK) are anchored in the postsynaptic membrane. Agrin, secreted into the synaptic space by the nerve terminal, binds to multiple sites on the extracellular domain of LRP4, which then binds to the extracellular domain of MuSK on the postsynaptic membrane. This results in phosphorylation and activation of MuSK and clustering of MuSK and LRP4.^{1,2} Activated MuSK, in concert with DOK7 and other postsynaptic proteins, acts on rapsyn to concentrate the acetylcholine receptor (AChR) in the postsynaptic membrane and promotes postsynaptic gene expression and differentiation. Clustered LRP4 also enhances presynaptic differentiation.³

Several reports have described congenital myasthenic syndromes (CMSs) caused by mutations in agrin⁴⁻⁶ and MuSK,⁷⁻¹¹ but only 1 report has described mutations in LRP4.¹² This was the case of a 14-year-old girl with moderately severe fatigable limb-girdle weakness, dysplastic synaptic contacts, borderline end-plate (EP) AChR deficiency, smaller-than-normal individual EP regions, but no demonstrable defect of neuromuscular transmission at intercostal muscle EPs. The patient's weakness continued to progress, and by 24 years of age, she was barely able to walk. Herein we describe 2 young adult sisters with LRP4-related myasthenia caused by a novel homozygous LRP4 mutation. Intercostal muscle studies of the older sister reveal structurally and functionally abnormal EPs and EP AChR deficiency. Expression studies indicate that the mutant protein hinders LRP4 from binding to, activating, and phosphorylating MuSK.

Methods

Participants

All human studies were approved by the institutional review board of the Mayo Clinic in Rochester, Minnesota, and the 2 sisters (ie, patients) and 15 historical control participants provided written informed consent to participate in the studies. Intercostal muscle was obtained from the 15 historical control participants during chest surgery for unrelated diseases.

Genetic Analysis

Sanger sequencing for mutations in genes known to cause limb-girdle CMS (namely, *RAPSN*, *DOK7*, *GFPT1*, and *DPAGT1*) gave negative results. Next, exome sequencing of genomic DNA from both siblings was performed at the Mayo Clinic. The identified putative variants were scrutinized with Ingenuity Variant Analysis software (Qiagen). Variants at intergenic and intronic sites, and genes not expressed in skeletal muscle or the spinal cord based on the Gene Expression Omnibus database (<http://www.ncbi.nlm.nih.gov/geo/>), were excluded. The identified mutation was confirmed by Sanger sequencing of the family. Nucleotides of *LRP4* complementary DNA (cDNA) were numbered according to GeneBank accession number NM_002334.3.

To determine whether an identified nucleotide variant caused abnormal splicing, we isolated cDNA from the muscle specimens obtained from control participants and the 2 patients. To detect any alternative transcript, we amplified the cDNA from exons 25 to 29 and exons 26 to 28 with primers designed for the cDNA of the 2 patients and 2 control participants.

Structural Studies

Intercostal and serratus anterior muscle specimens were obtained from the older sister and from control participants without muscle disease undergoing thoracic surgery. Cryosections were used to colocalize the AChR and acetylcholinesterase as previously described.¹³ End plates were localized for electron microscopy¹⁴ and quantitatively analyzed¹⁵ by established methods. Peroxidase-labeled α -bungarotoxin was used for the ultrastructural localization of AChR.¹⁶ The number of AChRs per EP was measured with iodine 125-labeled α -bungarotoxin.¹⁷

In Vitro Electrophysiology Studies

Quantitative analysis of single EP regions was done for all 15 control participants and microelectrode studies of neuromuscular transmission and α -bgt binding sites per EP was conducted for 13 control participants. Intracellular microelectrode studies were performed on an intercostal muscle specimen obtained from the 34-year-old sister (patient 1). The amplitude of the miniature EP potential (MEPP) and the quantal content of the EPP (*m*) were determined as previously described.¹⁸⁻²⁰

Plasmids

We used the following previously constructed plasmids: (1) full-length human *LRP4* cDNA for the luciferase assay and cell surface binding assays; (2) mouse *Musk* cDNA for luciferase assay; (3) the extracellular domain of mouse *Musk* cDNA and a fraction (amino acids 1141-1937) of rat *Agrin* cDNA, both of which were fused to an myc-tag and alkaline phosphatase (MuSKect-mycAP and agrin-mycAP) for cell surface binding assay; and (4) human *MUSK* cDNA with a flag-tag at the N-terminal end for coimmunoprecipitation assay. Mutant *LRP4* plasmid carrying p.Glu1233Ala was generated by the QuikChange Site-Directed Mutagenesis kit (Stratagene).¹² The ATF2-luciferase (ATF2-luc) reporter¹² and the phRL-TK Renilla luciferase vector (Promega) were used for the luciferase reporter assay.

Cell Cultures

HEK293 and COS7 cells were cultured in the Dulbecco Modified Eagle Medium supplemented with 10% fetal calf serum, and transfected with FuGENE 6 transfection reagent (Roche). The agrin-mycAP and MuSKect-mycAP proteins were produced as previously described.¹² Recombinant rat C-terminal agrin (10 ng/mL; R&D Systems) was used for agrin treatment, except for the cell-binding assays.

Luciferase Assays

We used an ATF2-luc reporter to monitor MuSK activation. The basis for this approach is that agrin induces JNK activation in myotubes²¹ and that a previous report²² has demonstrated in-

teraction between JNK and ATF2. This suggested that reporters regulated by JNK might reflect MuSK activation. We therefore tested several JNK reporters and found that ATF2-luc reporter responded to MuSK, LRP4, and agrin in a dose-dependent manner.¹²

HEK293 cells were transfected with ATF2-luc and phRL-TK along with the *MUSK* cDNA and the *LRP4* cDNA. Cells were cultured for 24 hours in a 96-well plate with or without 10 ng/mL of agrin in the medium. Cells were lysed with the Passive Lysis Buffer (Promega) and assayed for luciferase activity using the Dual-Luciferase Reporter Assay System (Promega). Each experiment was performed in triplicate.

Western Blotting

HEK293 cells transfected with MuSK and LRP4 plasmids were cultured for 24 hours in the presence of 10 ng/mL of agrin, as previously described.¹² The primary antibodies were mouse monoclonal anti-FLAG M2 (Sigma-Aldrich; F3165, dilution 1:4000), anti- β -actin (Santa Cruz Biotechnology; sc-47778, dilution 1:200), and the goat polyclonal anti-LRP4 (Abcam; ab85697, dilution 1:1000). The secondary antibodies were goat antimouse IgG (GE Healthcare; NA931V, dilution 1:6000) and mouse antigoat IgG (Santa Cruz Biotechnology; sc-2345, dilution 1:6000) conjugated to horseradish peroxidase.

Biotinylation Assay

HEK293 cells transfected with plasmids harboring wild-type LRP4 or its Glu1233Ala mutant were cultured for 48 hours. Cell surface proteins were isolated by biotinylating the cell surface proteins and precipitating the bound proteins with streptavidin beads, as previously described.¹²

Results

Clinical Data

Two young adult sisters with CMS (patient 1 in her mid-30s and patient 2 in her early 20s) who were born to nonconsanguineous parents, were investigated. Their parents and other siblings are unaffected.

Patient 1 was born after normal gestation and delivery. months. Developmental milestones (sitting and walking) were slightly delayed; after beginning to walk, she fell frequently. As a young child, she had mild difficulty chewing and swallowing. She never climbed steps or kept up with her peers in physical activities. Her weakness worsened around her menses. In her teens, she could only walk a short distance with support and became dependent on a wheelchair. On initial examination, she could barely rise from the sitting position without support, and her gait was waddling, hyperlordotic, and intoeing. Her weakness was confined to the axial and limb muscles with selective severe involvement of the dorsal forearm muscles. Her tendon reflexes were hypoactive. Her vital capacity was reduced to 49%, and the maximal inspiratory and expiratory pressures were reduced to 43% and 22% of normal, respectively. Repetitive nerve stimulation at 2 Hz revealed a decremental response of 37% in the trapezius and of 14% in facial muscles of the fourth compared with the first evoked compound muscle action potential

(CMAP) (normal, <10%). Repetitive CMAPs, typical of the slow-channel myasthenic syndrome or EP acetylcholinesterase deficiency,²³ were absent. Brief strenuous exercise did not appreciably improve the decremental response or potentiate the first evoked CMAP as in the CMS-caused synaptotagmin-2 deficiency,²⁴ in some patients harboring mutations in agrin,⁶ or in the Lambert-Eaton syndrome.²³ Needle electromyographic studies of multiple muscles revealed an increased proportion of short-duration, polyphasic motor unit potentials without spontaneous electrical activity, a common finding in myasthenic disorders owing to a variable proportion of muscle fibers in motor units failing to generate an action potential.

After treatment with 4 mg of albuterol sulfate twice daily for 1 week, patient 1 rose up from the sitting position 10 times without support, and the electromyographic decrement in her trapezius muscle decreased to 25%. One week later, she climbed 10 steps, walked 450 m (500 yd), and was able to groom herself independently. Additional treatment with pyridostigmine bromide or 3,4-diaminopyridine made her weaker and had to be discontinued.

Patient 2 appeared normal at birth and during infancy. She walked at a developmentally appropriate age but never learned to run or jump, found it difficult to climb steps, and could not keep up with her peers in physical activities. By late adolescence, her arm-elevation time was 22 seconds, and her gait was lordotic and waddling; she required assistance to rise from a sitting position and could climb only 20 steps before having to rest. There was mild weakness of the cervical and proximal arm muscles and mild to moderately severe weakness of the hip girdle muscles. Her tendon reflexes were hypoactive. Respiratory function tests showed that her vital capacity was reduced to 68% and that her maximal inspiratory and expiratory pressures were reduced to 39% and 47% of normal, respectively. After treatment with 4 mg of albuterol twice daily for 2 weeks, her arm and cervical muscles were of normal strength, her arm-elevation time was 60 seconds, and she could climb 44 steps before having to rest. Additional treatment with 60 mg of pyridostigmine twice daily over the next 2 years neither improved nor worsened her condition. A needle electromyographic examination suggested a mild proximal myopathy. After receiving albuterol for 2 years, repetitive stimulation of multiple muscles revealed no significant decrement of the evoked CMAP.

Structural Studies

Structural studies were performed in patient 1. Light microscopy revealed markedly diminished EP size. In transverse frozen sections reacted for acetylcholinesterase, the median length of 34 EPs was 7.2 μ m (Figure 1A, B, E, and F); the median length of 69 EPs of 3 control participants was 21.3 μ m ($P < .001$, determined by the use of the rank sum test) (Figure 1C, D, G, and H). Paired fluorescence localization studies revealed reduced synaptic expression of acetylcholinesterase and of the AChR in the EPs of patient 1 (Figure 1E and F) compared with the EPs in the 3 control participants (Figure 1G and H).

Qualitative inspection of 15 EP regions revealed 7 postsynaptic regions unoccupied or partially occupied by the nerve